A Global Sensitivity Analysis framework for guiding the design improvement of new concepts of Small Modular Reactors

Stefano Marchetti[a], Francesco Di Maio[a], Enrico Zio[b,a], Emanuele Borgonovo[c], Elmar Plischke[d]

[a]Energy Department, Politecnico di Milano, Milano 20156, Italy.

[b]MINES Paris-PSL, Centre de Recherche sur les Risques et les Crises (CRC), Sophia Antipolis, France.

[c]Department of Decision Sciences, Bocconi Institute for Data Science and Analytics, Bocconi University, 20136 Milan, Italy.

[d]Institute of Disposal Research, Clausthal University of Technology, 38678 Clausthal-Zellerfeld, Germany.

Abstract

Small Modular Reactors (SMRs) are new concepts of Nuclear Power Plants (NPPs) whose safety assessment typically cannot rely on design-specific operational experience and field data. Assessing their safety requires a careful combination of engineering expertise, and of physical (laboratory) and virtual (simulation) experiments. Modeling the system response accurately, in consideration of the engineering design and physical aspects of SMRs requires computationally burdensome computer models. Although interpretable, it is difficult to consistently identify the most important inputs and provide safety margins, especially for high-dimensional correlated inputs and outputs. To address these issues, we propose a Global Sensitivity Analysis (GSA) framework that combines recently introduced global sensitivity indices based on Optimal Transport (OT) with a graphical visualization tool based on CUmulative SUm of NOrmalized Reordered Output (CUSUNORO). The OT-based indices allow us to identify the most important inputs, whereas the graphical representation of the latter enables us to identify the safety critical ranges of these inputs. The proposed framework is applied to a demonstrative case study concerning Small Modular Dual Fluid Reactors (SMDFRs), a new SMR concept. The numerical experiments show how the approach can help interpreting the simulation results and suggesting design improvements to keep operational settings away from the Critical failure Region (CR).

Keywords: Small Modular Reactor (SMR), Safety Design, Critical failure Region (CR), Global Sensitivity Analysis (GSA), Optimal Transport (OT), CUmulative SUm of NOrmalized Reordered Output (CUSUNORO).

Acronyms

ACS	Auxiliary Cooling System
AFS	Auxiliary Feedwater System
AGAN	As Good As New
AGAO	As Good As Old
CDF	Cumulative Distribution Function
CP	Coolant Pipe
CR	Critical failure Region
CUSUNORO	CUmulative SUm of NOrmalized Reordered Output
EDG	Emergency Diesel Generator
GSA	Global Sensitivity Analysis
IUQ	Inverse Uncertainty Quantification
LBLOCA	Large Break Loss Of Coolant Accident
LOCA	Loss Of Coolant Accident
LOP	Loss Of Power
LWR	Light Water Reactor
MFP	Melting Fuel Plug
MSR	Molten Salt Reactor
MU	Multi-Unit
NPP	Nuclear Power Plant
NRC	Nuclear Regulatory Commission
OT	Optimal Transport
PGA	Peak Ground Acceleration
PoF	Physics of Failure
PPU	Pyrochemical Processing Unit
PSA	Probabilistic Safety Assessment
PSM	Probabilistic Safety Margin
SMDFR	Small Modular Dual Fluid Reactor
SMR	Small Modular Reactor

Symbols

N	Number of nuclear reactor units
T_w	Peak cladding temperature
n	Index of reactor unit
$\boldsymbol{X}$	Model inputs
I	Number of model inputs
$\boldsymbol{Y}$	Model outputs
O	Number of model outputs
$\mathbb{P}_{\boldsymbol{X}}$	Probability distribution of input values
$\mathbb{P}_{\boldsymbol{Y}}$	Probability distribution of output values
$\boldsymbol{y}_{thres}$	Output threshold values
$\boldsymbol{x}_{crit}$	Input critical values
$\xi(\boldsymbol{Y}, X_i)$	Global sensitivity measure of X_i with respect to $\boldsymbol{Y}$
$\zeta\left(\mathbb{P}_{\boldsymbol{Y}}, \mathbb{P}_{\boldsymbol{Y}\|X_i}\right)$	Distance between $\mathbb{P}_{\boldsymbol{Y}}$ and $\mathbb{P}_{\boldsymbol{Y}\|X_i}$
$f_i(X_i)$	Probability density function of X_i
$i(\boldsymbol{Y}, X_i)$	OT-based sensitivity index
$\pi(\boldsymbol{y}, \boldsymbol{y}')$	Transport plan from $\mathbb{P}_{\boldsymbol{Y}}$ to $\mathbb{P}_{\boldsymbol{Y}\|X_i}$
$k(\boldsymbol{y}, \boldsymbol{y}')$	Cost for moving a value that follows $\mathbb{P}_{\boldsymbol{Y}}$ to a value that follows $\mathbb{P}_{\boldsymbol{Y}\|X_i}$
$K(\pi)$	Integral cost given plan $\pi(\boldsymbol{y}, \boldsymbol{y}')$
$d^p(\boldsymbol{y}, \boldsymbol{y}')$	Euclidean distance between realizations of $\mathbb{P}_{\boldsymbol{Y}}$ and $\mathbb{P}_{\boldsymbol{Y}\|X_i}$
$W_p^p(\nu, \nu_i)$	*p-th* power of the Wasserstein distance of order p
$i^{WB}(\boldsymbol{Y}, X_i)$	Wasserstein-Bures metric
Γ	Residual term of OT-based sensitivity index
$\mathbb{P}_{\boldsymbol{Y}\|X_i}$	Probability distribution of output values conditioned on x_i
$\mathbb{E}[\cdot]$	Expected value operator
$\mathbb{V}[\cdot]$	Variance operator
$Adv(\boldsymbol{Y}, X_i)$	Advective component of $i^{WB}(\boldsymbol{Y}, X_i)$
$Diff(\boldsymbol{Y}, X_i)$	Diffusive component of $i^{WB}(\boldsymbol{Y}, X_i)$
$\Sigma_{\boldsymbol{Y}}$	Second moment of the output distribution
$\Sigma_{\boldsymbol{Y}\|X_i}$	Second moment of the output distribution conditioned on x_i
C^{bf}	Double loop Monte Carlo computational cost
N_{out}	Sample size of outer Monte Carlo loop

N_{in}	Sample size of inner Monte Carlo loop
C^{sim}	Given-data approach computational cost
N_{sim}	Number of simulations of the available dataset
π	Permutation
$z_o(i)$	CUSUNORO for input x_i
$\overline{y_o}$	Expected value of the *o-th* output
$y_{\gamma,o}$	γ-percentile of the *o-th* output
PSM_o	PSM of the *o-th* output
$y_{nom,o}$	Nominal value of the *o-th* output
$\boldsymbol{X}^*$	Inputs most impacting the SMR safety
$T_{w,nom}$	Nominal peak cladding temperature
$\dot{m}_{leak}$	LOCA leak mass flow rate
t^r	Safety feature response time
Δt_m	Time interval between two maintenance interventions
t_{ACS}^{mean}	Mean value of ACS failure time
t_{EDG}^{mean}	Mean value of EDG failure time
$U(\cdot)$	Uniform probability distribution
$N(\cdot)$	Normal probability distribution
d_{in}	Initial depth of corrosion defect
t^f	Safety feature failure time
T_s	Simulation time
$T_{w,fail}$	Threshold cladding temperature
E	Young modulus
γ	Coefficient of thermal expansion
σ	Tensile strength
$T_{w,max}$	Maximum value of T_w during the accidental scenario
N_{sim}^{total}	Total number of simulations
PGA_{single}^{median}	Median PGA value leading to a single LOCA
$PGA_{multiple}^{median}$	Median PGA value leading to multiple LOCAs
$N_{sim,2}$	Number of simulated accidental scenarios with imperfect maintenance
τ_E^q	Effective age after the *q-th* maintenance intervention
α	Effectiveness of maintenance

$t_{ACS,crit}^{f}$	Critical value of ACS failure time
PGA_{crit}	Critical value of PGA
μ	Median seismic capacity
β	Standard deviation of logarithmic median seismic capacity
$\phi(\cdot)$	Standard normal cumulative distribution function
D	Damping coefficient
PGA_{BDBE}	PGA corresponding to a beyond design basis earthquake
$P_{F,s}$	Failure probability of the *s-th* safety feature
$P_{F,s}^{*}$	Failure probability of the *s-th* safety feature considering the design improvements
N_{sim}^{*}	Number of simulated accidental scenarios with the design improvements
$F_{P,n}$	Failure probability of the *n-th* reactor unit

1. Introduction

Small Modular Reactors (SMRs) promise lower construction and operational costs, enhanced safety features with respect to traditional large-scale Nuclear Power Plants (NPPs) [1], and flexible power capacity through modular Multi-Unit (MU) configurations [2]. To achieve safety enhancements, the design of SMRs must prioritize safety since the very early stages, implementing comprehensive defense-in-depth strategies for preventing severe accidents and mitigating their consequences [3]. In this regard, a rigorous assessment of the Critical failure Region (CR), i.e., the boundary of the reactor parameter space beyond which failure may lead to unacceptable consequences [4], is needed to risk-inform the effective deployment of defense-in-depth principles.

Because of the lack of operational experience and data, the risk-informed design process requires relying on complex, high-fidelity simulators to replicate as realistically as possible the physics and thermodynamics of SMRs, and obtain reliable indications of their behavior during accidents. However, the lack of data implies uncertainty in the input parameters of the simulation codes, which reverberates on their output results. One, then, needs to perform thorough uncertainty quantification to characterize the variability in the safety-related quantities of interest by propagating input uncertainties through the simulators ([5], [6]). At the same time, it is important, especially for SMRs, to identify key inputs and ensure adequate safety margins, given the complexity of the physical models involved ([7], [8]). In this respect, the literature has demonstrated that integrating uncertainty quantification with sensitivity analysis can, in fact, meet these needs [9].

Sensitivity analysis methods are typically classified into local and global. Local sensitivity analysis evaluates the impact of variations in one or more inputs at a specific location in the input parameter space. Local methods comprise differentiation-based methods or methods based on finite differences. An early discussion in the nuclear industry is offered by ([10], [11]). As seen in the literature, local techniques are not designed to capture uncertainty. Also, they typically imply the variation of one-input-at-a-time, thus failing in capturing or respecting input dependences. This makes them possibly less suitable for inferring the importance of inputs in complex and nonlinear models, which, instead, are common in SMR simulations [12]. Conversely, GSA methods are designed to allow the input parameters to vary across their full ranges and account for interactions and nonlinearities [12]. GSA has already been applied across various disciplines in the nuclear sector and as well as in climate change [13], socio-cultural [14], thermal [15] and mechanical [16] models. In the nuclear industry, applications involve identifying surrogate model parameters [17], tailoring Inverse Uncertainty Quantification (IUQ) processes [18], analyzing source term uncertainties in accidental scenarios [19], and evaluating the time-dependent effects of uncertain parameters on reactor cladding temperatures

during Large Break Loss Of Coolant Accidents (LBLOCAs) [20]. Additionally, sensitivity analysis, such as perturbation-theory-based approaches [21], is integral to the Best Estimate Plus Uncertainty method, widely adopted for NPPs safety assessments [22].

Applying GSA methods to SMR simulators introduces new challenges and opens new research questions. First, the analysis is challenging, because of the large computational burden of the simulation codes, which calls for an extensive uncertainty quantification that allows modelers to inspect the model behavior thoroughly, letting the inputs vary simultaneously in the parameter space. This is necessary to properly characterize engineering uncertainty in the safety-related quantities of interest ([23], [24]). Second, SMR models typically output a multiplicity of quantities of interest, while most GSA methods in use are constructed for univariate responses [25]. Third, inputs might be correlated, which is also a challenge for current GSA methods.

To solve these issues, we propose a novel framework that combines input prioritization through Optimal Transport (OT)-based sensitivity indices [25], and the assessment of marginal behavior through the CUmulative SUm of NOrmalized Reordered Output (CUSUNORO) [26]. OT-based global sensitivity indices are defined to yield the importance of inputs for univariate or multivariate outputs and are well posed in the presence of correlated inputs. Through CUSUNORO curves, one can perform a critical parameter segmentation, i.e., identify the critical input values, that, if exceeded, may cause the system to quickly approach the CR. The novelty of the approach lies in the integrated use of a suite of SA approaches, i.e., OT-based sensitivity indices and CUSUNORO, to enable decision support regarding the design of new concepts of NPPs, such as SMRs.

Regarding the computational burden, both OT and CUSUNORO are calculated with a given-data approach using a single-loop Monte Carlo estimation, i.e., directly from the simulations used for uncertainty quantification [27]. If N_{sim} denotes the number of simulations used for uncertainty quantification, then the computational cost of the method is N_{sim}, making it independent of the input dimensionality. Conceptually, this is the minimal cost for GSA. Thus, the method post-processes the input-output dataset produced by a Monte Carlo uncertainty analysis. Consequently, as it happens in any GSA investigation, the quality of the results is associated with the uncertainty quantification thoroughness, as an insufficient exploration of the input-output space might affect the reliability of the analysis.

We present the implementation of the proposed method first through a simple analytical example. We, then, tackle a demonstrative test case, based on a MU-SMR installation composed by $N = 4$ units of Small Modular Dual Fluid Reactor (SMDFR), a fast reactor design with liquid lead flowing through the reactor core as coolant and molten salt as fuel [28]. The high operating temperatures that

can be reached ensure a high thermal efficiency and make the SMDFR ideal for clean hydrogen production [29]. The overall design has four shared Auxiliary Cooling Systems (ACSs) to provide additional coolant mass flow rate to the SMDFR coolant circuit in case of Loss Of Coolant Accident (LOCA), and two shared Emergency Diesel Generators (EDGs) to operate in case of Loss Of Power (LOP). A simulation model is used to assess the NPP response to accidental scenarios initiated by an earthquake [30]. The model accounts for both the inter-unit dependencies among the different units and for the age-dependent fragility of the safety features (ACSs, EDGs and reactors Coolant Pipes (CPs)). The peak cladding temperature (T_w) is the safety-related quantity of interest [30]. Parameter prioritization by OT lists the earthquake Peak Ground Acceleration (PGA), the corrosion of CP and the failure time of ACS as the most important inputs. The results of the OT-based sensitivity provide effective indications for design improvement, e.g., improving the seismic reliability of the NPP and the resistance to corrosion of CP. The CUSUNORO analysis provides, in addition, insights on the failure-critical values of these parameters, which can be used to ensure that the SMDFR operates far from the CR.

The remainder of the paper is organized as follows: Section 2 describes the sensitivity analysis methods used in the work; Section 3 illustrates the proposed GSA framework; Section 4 presents the case study and the results of the application of the proposed framework; Section 5 offers conclusions.

2. The sensitivity analysis methods

Out approach is based on the combination of global sensitivity indices based on the theory of optimal transport and CUSUNORO curves. Section 2.1 presents the general GSA setup. Sections 2.2 and 2.3 present OT-based global sensitivity measures and the CUSUNORO method, respectively.

2.1. Setup

In the general GSA setup, one considers a simulation model that processes a set of inputs and calculates a set of quantities of interest. We denote the vector of inputs and outputs respectively by $\boldsymbol{X} = [X_1, X_2, \dots, X_I] \in D_{\boldsymbol{X}} \subset \mathbb{R}^I$, and $\boldsymbol{Y} = [Y_1, Y_2, \dots, Y_O] \in D_{\boldsymbol{Y}} \subset \mathbb{R}^O$, where I and O are the number of inputs and outputs. We also let $\boldsymbol{Y} = m(\boldsymbol{X})$ denote the input-output mapping, with $m: D_{\boldsymbol{X}} \rightarrow D_{\boldsymbol{Y}}$. Under uncertainty, the inputs and outputs are random variables on measurable space $(\Omega, B(\Omega), \mathbb{P})$, with joint probability law $\mathbb{P}_{\boldsymbol{Y},\boldsymbol{X}}$ and marginal distributions $\mathbb{P}_{\boldsymbol{X}}$ and $\mathbb{P}_{\boldsymbol{Y}}$, respectively. We also assume that the conditional laws $\mathbb{P}_{\boldsymbol{Y}|X_i}$ are well posed for all $i = 1,2, \dots, I$. Throughout the paper, we will assume that the model output has finite second order moment. This implies that the variance of Y_o is finite, an assumption that is verified by physical systems.

Under uncertainty, knowledge about the key-factors that drive the model response is gained through GSA methods. These methods have a long tradition and several of them have been developed to address problems originated by nuclear engineering applications. We recall the work of [31], that describes the risk and uncertainty analysis for dose exposure from radioactive waste disposals, of [32], that uses importance measures for the performance assessment of a nuclear waste repository and of [33], where GSA is applied to fuel performance codes.

Several of the GSA methods in use can be encompassed in a common rationale, where one writes the global sensitivity measure of X_i with respect to $\boldsymbol{Y}$ as [34]:

$$\xi(\boldsymbol{Y}, X_i) = \mathbb{E}\left[\zeta\left(\mathbb{P}_{\boldsymbol{Y}}, \mathbb{P}_{\boldsymbol{Y}|X_i}\right)\right], \tag{1}$$

where $\zeta\left(\mathbb{P}_{\boldsymbol{Y}}, \mathbb{P}_{\boldsymbol{Y}|X_i}\right)$ is a distance (or separation) between the probability distribution of $\boldsymbol{Y}$ and its conditional probability distribution after learning X_i and the expectation is carried over the distribution of X_i. To illustrate, if X_i is an absolutely continuous random variable, denoting its probability density function with $f_i(X_i)$, then Eq. (1) is equivalent to:

$$\xi(\boldsymbol{Y}, X_i) = \int_{-\infty}^{\infty} \zeta\left(\mathbb{P}_{\boldsymbol{Y}}, \mathbb{P}_{\boldsymbol{Y}|X_i}\right) f_i(X_i) dX_i \tag{2}$$

Variance-based sensitivity measures are encompassed by the common rationale. To illustrate, if the output is univariate and we select as a separation measurement the quantity

$$\zeta^{VB}\left(\mathbb{P}_{Y}, \mathbb{P}_{Y|X_i}\right) = \frac{(\mathbb{E}[Y|X_i] - \mathbb{E}[Y])^2}{\mathbb{V}[Y]} \tag{3}$$

we obtain $\xi^{VB}(Y, X_i)$, given by:

$$\xi^{VB}(Y, X_i) = \frac{\mathbb{V}[Y] - \mathbb{E}_{X_i}\left[\mathbb{V}_{X_{j\neq i}}[Y|X_i]\right]}{\mathbb{V}[Y]} = S(Y, X_i) \tag{4}$$

The variance-based index $\xi^{VB}(Y, X_i)$ coincides with the first-order variance-based indices, also known as Sobol indices. When inputs are dependent, Eq. (4) is equivalent to Pearson correlation ratio and coincides with the global sensitivity measure proposed by [35] for the probabilistic risk assessment of NPPs.

However, these methods have been developed mainly for univariate quantities of interest and are challenged by the multivariate nature of the simulation output, which, instead, characterizes the simulations of SMRs, especially when they are time or space dependent. To solve this issue, we rely on a global sensitivity measure based on the theory of optimal transport that we discuss in Section 2.2.

2.2. Optimal Transport-based GSA

The global sensitivity measure we use in this work has been defined in [25], to which we refer for a complete overview. To make the present paper self-contained, we offer a concise overview. The theory of optimal transport has been widely studied across mathematics, statistics and machine learning [36]. A detailed theoretical description of can be found in ([37], [38]). Of relevance to us is the use of optimal transport to measure the distance between probability distributions.

In our context, we are considering two distributions of $\boldsymbol{Y}$, its marginal distribution $\mathbb{P}_{\boldsymbol{Y}}$ and conditional distribution $\mathbb{P}_{\boldsymbol{Y}|X_i}$. For notation simplicity, let us denote them with $\nu = \mathbb{P}_{\boldsymbol{Y}}$ and $\nu_i = \mathbb{P}_{\boldsymbol{Y}|X_i}$, respectively. In an optimal transport setting, we aim to find a transport plan from ν to ν_i that minimized a given cost function. We denote a generic transport plan with $\pi(\boldsymbol{y}, \boldsymbol{y}')$, where $\boldsymbol{y}$ and $\boldsymbol{y}'$ are realizations, respectively, of $\boldsymbol{Y}$ and $\boldsymbol{Y}'$. Note that $\pi(\boldsymbol{y}, \boldsymbol{y}')$ is a function mapping $k: D_{\boldsymbol{Y}} \times D_{\boldsymbol{Y}} \rightarrow [0, +\infty]$ that gives us the cost $k(\boldsymbol{y}, \boldsymbol{y}')$ we incur for moving a value of $\boldsymbol{y}$ that follows the distribution ν to a value $\boldsymbol{y}'$ that follows the conditional distribution ν_i.

The choice of the cost function can be quite general. As in [25], a typical choice is for $k(\boldsymbol{y}, \boldsymbol{y}')$ to be lower semi-continuous. Then, the integral cost given plan $\pi(\boldsymbol{y}, \boldsymbol{y}')$ is:

$$K(\pi) = \iint_{Y \times Y} k(\boldsymbol{y}, \boldsymbol{y}')\, d\pi(\boldsymbol{y}, \boldsymbol{y}') \tag{5}$$

The Kantorovich OT-problem is then to find the plan $\pi(\boldsymbol{y}, \boldsymbol{y}')$ that minimizes $K(\pi)$. There is a high flexibility in choosing the cost function. A typical choice is the Euclidean distance, so that $k(\boldsymbol{y}, \boldsymbol{y}') = d^p(\boldsymbol{y}, \boldsymbol{y}') = \|\boldsymbol{y} - \boldsymbol{y}'\|^d$. In this case, the OT-problem becomes to determine

$$W_p^p(\nu, \nu_i) = \inf_{\pi \in \Pi(\nu, \nu_i)} \int d^p(\boldsymbol{y}, \boldsymbol{y}')\; d\pi(\boldsymbol{y}, \boldsymbol{y}') \tag{6}$$

where $W_p^p(\nu, \nu_i)$ is the *p-th* power of the so-called Wasserstein distance of order p between ν and ν_i. When $p = 2$, we find the 2-squared Wasserstein distance

$$W_2^2(\nu, \nu_i) = \inf_{\pi \in \Pi(\nu, \nu_i)} \int \|\boldsymbol{y} - \boldsymbol{y}'\|^2 d\pi(\boldsymbol{y}, \boldsymbol{y}') \tag{7}$$

which has been widely studied and applied in the literature. $W_2^2(\nu, \nu_i)$ admits a decomposition into three distinct components, which turns out to be convenient for GSA ([39], [40]). We have:

$$W_2^2(\nu, \nu_i) = \|\mathbb{E}[\boldsymbol{Y}] - \mathbb{E}[\boldsymbol{Y}|X_i]\|^2 + Tr\left(\Sigma_{\boldsymbol{Y}} + \Sigma_{\boldsymbol{Y}|X_i} - 2\Sigma_{\boldsymbol{Y}}^{1/2}\Sigma_{\boldsymbol{Y}|X_i}\Sigma_{\boldsymbol{Y}}^{1/2}\right) + \Gamma(\nu, \nu_i) \tag{8}$$

where:

- $\mathbb{E}[\boldsymbol{Y}]$ and $\mathbb{E}[\boldsymbol{Y}|X_i]$ are, respectively, the expected value of $\boldsymbol{Y}$ and the conditional expected value of $\boldsymbol{Y}$ given X_i. The term $\|\mathbb{E}[\boldsymbol{Y}] - \mathbb{E}[\boldsymbol{Y}|X_i]\|^2$ quantifies the contribution due to the difference in the marginal and conditional expected values of $\boldsymbol{Y}$.
- $\Sigma_{\boldsymbol{Y}}$ and $\Sigma_{\boldsymbol{Y}|X_i}$ are the corresponding variance-covariance matrices, and the matrix trace term (i.e., $Tr\left(\Sigma_{\boldsymbol{Y}} + \Sigma_{\boldsymbol{Y}|X_i} - 2\Sigma_{\boldsymbol{Y}}^{1/2}\Sigma_{\boldsymbol{Y}|X_i}\Sigma_{\boldsymbol{Y}}^{1/2}\right)$) quantifies the difference in the second-order (covariance) structure.
- The term $\Gamma(\nu, \nu_i)$ quantifies the difference in the two distributions due to the effect of higher-order moments. $\Gamma(\nu, \nu_i)$ becomes null if ν and ν_i are two distributions belonging to the elliptical distribution family with the same characteristic generator [40]. This is the case when both the marginal and the conditional distribution of $\boldsymbol{Y}$ are Gaussian.

The work of [25] defines the following global sensitivity measure based on the square 2-Wasserstain distance:

$$i(\boldsymbol{Y}, X_i) = \frac{\mathbb{E}\left[W_2^2\left(\mathbb{P}_{\boldsymbol{Y}}, \mathbb{P}_{\boldsymbol{Y}|X_i}\right)\right]}{2\mathbb{V}[\boldsymbol{Y}]}, \tag{9}$$

where $\mathbb{V}[\boldsymbol{Y}]$ is the variance of $\boldsymbol{Y}$, which, in a multivariate context, is the sum of the univariate variances of the outputs, that is, $\mathbb{V}[\boldsymbol{Y}] = \sum_{o=1}^{O} \mathbb{V}[Y_o]$. The global sensitivity index $i(\boldsymbol{Y}, X_i)$ possesses relevant properties [25], whose importance is highlighted in recent statistical literature [41]:

- zero-independence: $i(\boldsymbol{Y}, X_i) = 0$ if and only if $\boldsymbol{Y}$ and X_i are statistically independent, ensuring that no important input is wrongly neglected in the analysis;
- max-functionality: $i(\boldsymbol{Y}, X_i) = 1$ if and only if $\boldsymbol{Y}$ is functionally dependent on X_i;
- monotonicity: $i(\boldsymbol{Y}, X_i)$ decreases if less refined information on X_i is received.

Zero-independence reassures us that if $i(\boldsymbol{Y}, X_i)$ is null then $\boldsymbol{Y}$ and X_i are statistically independent, that is, when fixing X_i does not change the distribution of $\boldsymbol{Y}$. Variance-based GSA methods do not satisfy this condition, because it may occur that $\boldsymbol{Y}$ and X_i are statistically dependent even if the value of the variance-based sensitivity measure is zero (see the notable example of the Ishigami function [42]). The max-functionality property looks at the maximum value of $\boldsymbol{Y}$ and guarantees that $i(\boldsymbol{Y}, X_i) = 1$ if and only if $\boldsymbol{Y}$ is functionally dependent only on X_i (i.e., $\boldsymbol{Y}$ is completely determined by fixing X_i). This gives the following interpretation of the values of $i(\boldsymbol{Y}, X_i)$: $0 \leq i(\boldsymbol{Y}, X_i) \leq 1$, with zero achieved when $\boldsymbol{Y}$ is not (statistically) affected by X_i and it is maximal if X_i determines $\boldsymbol{Y}$ completely. This allows a straightforward interpretation of the value of $i(\boldsymbol{Y}, X_i)$ and a transparent way to rank the inputs. Also, $i(\boldsymbol{Y}, X_i)$ is well-defined and interpretable even when the inputs are correlated. This is

because it does not rely on decomposing the output variance into contributions of independent inputs, but rather it quantifies how much the distribution of $\boldsymbol{Y}$ changes given X_i.

Formally, the index in Eq. (9) is a moment-independent sensitivity measure, because it measures the separation between two distributions without any reference to its moments. However, the decomposition in Eq. (8) allows us to connect the moment independent index to contributions related to the expected impact of fixing X_i on the variance and higher order moments of $\boldsymbol{Y}$. Substituting the decomposition in Eq. (8) into Eq. (9) yields:

$$i(\boldsymbol{Y}, X_i) = i^{VB}(\boldsymbol{Y}, X_i) + i^{\Sigma}(\boldsymbol{Y}, X_i) + \frac{\mathbb{E}\left[\Gamma\left[\mathbb{P}_{\boldsymbol{Y}}, \mathbb{P}_{\boldsymbol{Y}|X_i}\right]\right]}{2\mathbb{V}[\boldsymbol{Y}]}, \tag{10}$$

where

$$i^{VB}(\boldsymbol{Y}, X_i) = \frac{\mathbb{E}[\|\mathbb{E}[\boldsymbol{Y}] - \mathbb{E}[\boldsymbol{Y}|X_i]\|^2]}{2\mathbb{V}[\boldsymbol{Y}]} = \frac{\sum_{o=1}^{O} S(Y_o, X_i)}{2}, \tag{11}$$

and

$$i^{\Sigma}(\boldsymbol{Y}, X_i) = \frac{\mathbb{E}\left[Tr\left(\left(\Sigma_{\boldsymbol{Y}} + \Sigma_{\boldsymbol{Y}|X_i} - 2\left(\Sigma_{\boldsymbol{Y}|X_i}^{\frac{1}{2}} \Sigma_{\boldsymbol{Y}} \Sigma_{\boldsymbol{Y}|X_i}^{\frac{1}{2}}\right)^{\frac{1}{2}}\right)\right)\right]}{2\mathbb{V}[\boldsymbol{Y}]} \tag{12}$$

The term $i^{VB}(\boldsymbol{Y}, X_i)$ is the sum of the variance-based indices of X_i to all outputs: thus, it accounts for the impact of X_i on the model outputs variance. The term $i^{\Sigma}(\boldsymbol{Y}, X_i)$ is the expected impact on the variance-covariance matrix of the output $\boldsymbol{Y}$, and the last term in Eq. (10) is the residual error term that contains the contribution to higher-order moments. Thus, $i(\boldsymbol{Y}, X_i)$ subsumes variance-based sensitivity indices. For this reason, summing $i(\boldsymbol{Y}, X_i)$ does not yield a value of 1, because also higher order contributions are included in its value.

A detailed description of the available given-data procedures to estimate $i(\boldsymbol{Y}, X_i)$ can be found in [25]. We note here that the suggested approach is based on a given-data strategy that allows one to obtain the estimates directly from the dataset provided for a Monte Carlo uncertainty quantification, performing the following steps, also shown in the flowchart of **Fig. 1**, for each input X_i:

1. sort the values of X_i in ascending order;
2. divide the sorted values of X_i into $h = 1,2, \dots, H$ intervals;
3. for each *h-th* interval, compute the optimal transport problem between the original data $\boldsymbol{Y}$ and the subset data $\boldsymbol{Y}_h$ corresponding to the selected interval, as follows:

a. if $\boldsymbol{Y}$ is univariate, the solution is exact and computationally efficient. The corresponding algorithm is based on sorting ([25], [43]);
b. if $\boldsymbol{Y}$ is multivariate, the OT problem can be solved exactly using the simplex algorithm or any of its specialized variants ([44], [45]);
c. if $\boldsymbol{Y}$ is multivariate and the number of available simulations is large, the OT problem can be solved approximately with the Sinkhorn algorithm, which is used in this paper. Such algorithm notably reduces the computational burden and makes the estimation feasible also for complex simulators [46];

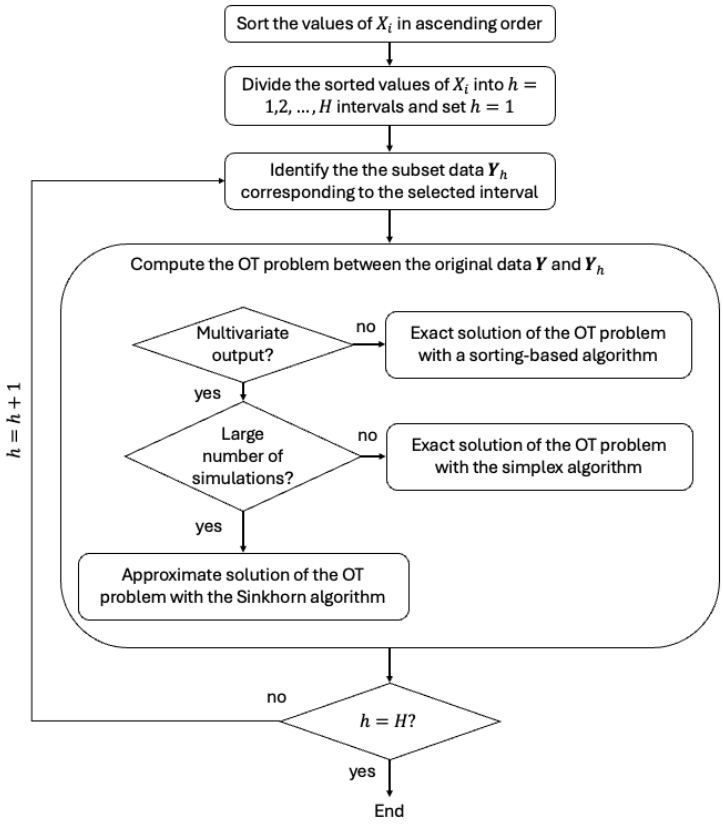

Fig. 1. Flowchart of the given-data procedure to estimate $i(\boldsymbol{Y}, X_i)$.

2.3. CUSUNORO-based graphical visualization tool

Let π denote a permutation that sorts the observed values of the *i-th* input X_i in ascending order, so that $x_{i,\pi(k)} \leq x_{i,\pi(k+1)}$, for all $k = 1,2,\dots,K-1$, where K is the number of observations for X_i. The CUSUNORO index, which has been introduced in [26], with respect to the *i-th* input and the *o-th* output is defined as follows:

$$z_o(i) = \frac{1}{\sqrt{I \cdot \sum_{k=1}^{K} \left(y_{o,k} - \overline{y_o}\right)^2}} \cdot \sum_{l=1}^{k} \left(\overline{y_o} - y_{o,\pi(l)}\right) \tag{13}$$

where $\overline{y_o}$ is the expected value of the *o-th* output. Sorting the output values $y_{o,\pi(l)}$ according to the sorted inputs and computing the cumulative sum of deviations from $\overline{y_o}$, $z_o(i)$ provides insights on the trend of the *o-th* output values due to with variations in the *i-th* input. A large cumulative sum $\sum_{l=1}^{k}(\overline{y_o} - y_{o,\pi(l)})$ indicates a strong influence of the *i-th* input on the *o-th* output, while fluctuations around zero mean weak or no influence. The resulting CUSUNORO plot, which plots $z_o(i)$ against the reordered input $x_{i,\pi(k)}$, helps to catch the trend visually. The following insights can also be drawn from a generic *i-th* CUSUNORO curve:

- sign of input-output dependency: if $z_o(i) > 0$, Y_o is directly proportional to X_i, if $z_o(i) < 0$, Y_o is inversely proportional to X_i, and if $z_o(i)$ crosses the horizontal axis multiple times, the dependency is non-monotonic;
- type of monotonic input-output dependency: the dependency is linear if the maximum absolute value of $z_o(i)$ occurs at the median of X_i, and nonlinear the further the maximum value from the median of X_i.

In case of monotonic nonlinear dependencies, the CUSUNORO plot can provide useful insights on the regions of large output sensitivity to inputs variations by highlighting, for each *i-th* input and *o-th* output, the corresponding critical input value $x_{i,crit}^{o}$, i.e., the value providing the maximum absolute value of $z_o(i)$, above (or below) which Y_o shows a highly nonlinear growth (decrease), which may cause the system to quickly approach the CR. We use Probabilistic Safety Margins (PSMs) to evaluate, in probabilistic terms, to which extent the outputs $\boldsymbol{Y}$ are below the thresholds $\boldsymbol{y}_{thres}$ (i.e., how far the system is from the CR) [47]; this is done by estimating, for each *o-th* output, the γ-percentile of its distribution (i.e., $y_{\gamma,o}$) and calculating the PSM as [48]:

$$PSM_o = \begin{cases} \dfrac{y_{thres,o} - y_{\gamma,o}}{y_{thres,o} - y_{nom,o}} & if\ y_{\gamma,o} \leq y_{thres,o} \\ 0 & if\ y_{\gamma,o} > y_{thres,o} \\ 1 & if\ y_{\gamma,o} < y_{nom,o} \end{cases} \tag{14}$$

where $y_{nom,o}$ is the nominal value of Y_o. The design improvements should, then, aim at maximizing the PSM_o, ensuring that X_i remains below (or above) $x_{i,crit}^{o}$ to prevent the nonlinear growth of Y_o, which would lead to a rapid decrease of PSM_o.

3. The proposed GSA framework

In this Section, we discuss the workflow of the methodology proposed in the paper. Let us consider a multivariate simulation model $\boldsymbol{Y} = m(\boldsymbol{X})$ of a safety-critical system, for which a dataset of N_{sim} simulations is assumed to be available. The system design should ensure that the SMR operates away

from the region of input values that lead to failure, i.e., the Critical Region $CR = \{\boldsymbol{x} \in D_{\boldsymbol{X}} \subset \mathbb{R}^I : \boldsymbol{y} = m(\boldsymbol{x}) \geq \boldsymbol{y}_{thres}\}$, where $\boldsymbol{y}_{thres} = [y_{thres,1}, y_{thres,2}, \dots, y_{thres,O}] \in D_{\boldsymbol{Y}} \subset \mathbb{R}^O$ is the vector of output thresholds that, if exceeded, lead the system into a failure state [4], and, thus, are typically defined by regulatory requirements or engineering safety standards. The proposed GSA framework consists of the following steps, also shown in the flowchart of **Fig. 2**:

- parameter prioritization by OT-based GSA; we identify the parameters that impact the SMR safety the most (i.e., the sub-vector $\boldsymbol{X}^* = [X_1^*, X_2^*, \dots, X_{I^*}^*]$ of the I^* (with $I^* < I$) inputs with the largest values of $i(\boldsymbol{Y}, X_i)$);
- critical parameters segmentation of the most important inputs by CUSUNORO, to identify the input critical values $\boldsymbol{x}_{crit} = [x_{crit,1}, x_{crit,2}, \dots, x_{crit,I^*}]$;
- identification of suitable design improvements to keep $\boldsymbol{X}^*$ far away from $\boldsymbol{x}_{crit}$.

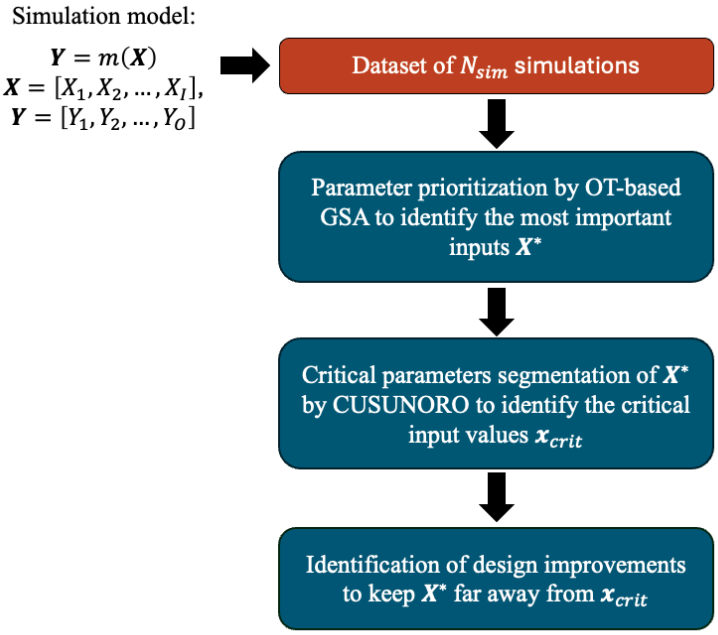

Fig. 2. Flowchart of the proposed GSA framework.

To illustrate the proposed framework, we consider the following analytic model:

$$(Y_1, Y_2) = m(X_1, X_2, X_3), \text{ with}$$
$$\begin{cases} Y_1 = -1.5\sqrt[5]{X_1} + X_2^4 + 0.01X_3 \\ Y_2 = X_1^2 + 2X_2 - 0.5X_3 \end{cases} \quad (15)$$

where $X_i \sim U(0,1)$. We select this example for the ease of interpretation, although it has no direct reference to a nuclear system. We assume that the analyst has performed an uncertainty quantification and has available an input-output dataset of $N_{sim} = 10^4$ simulations. The procedure described in Section 2.2 is used to estimate $i(\boldsymbol{Y}, X_i)$. The results are reported in **Fig. 3**.

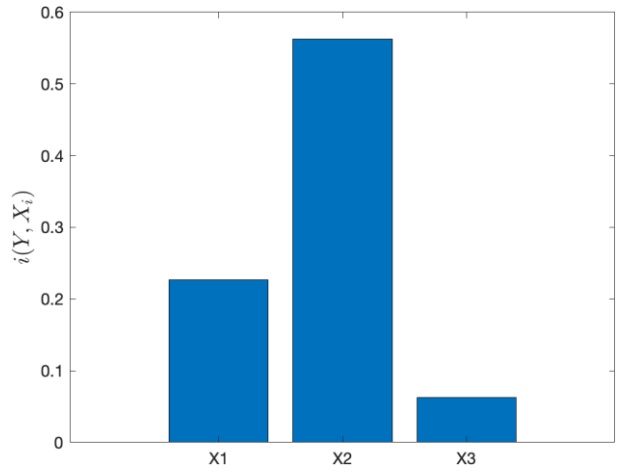

Fig. 3. OT results for the analytic function in Eq. (15).

Fig. 3 shows that X_2 is the most relevant input, followed by X_1 and with X_3 playing a minor role. The design improvements of a system modelled by Eq. (15), whose parameters are X_1, X_2 and X_3, should, thus, focus on X_2 and X_1 rather than X_3.

For the sake of brevity, in what follows we only consider the first output (i.e., Y_1) with $y_{thres,1} = 0.2$, $y_{nom,1} = -1.25$ and $\gamma = 95$, leading to $PSM_Y = 0.40$. Then, following the insights provided by the OT-based parameter prioritization, $z_o(i)$ is calculated with Eq. (13) only for X_1 and X_2, and the corresponding CUSUNORO curves are plotted against their empirical Cumulative Distribution Function (CDF) (i.e., CDF_i $i = 1,2$) in **Fig. 4** and **Fig. 5**, respectively; analyzing the curves, the following considerations can be drawn:

- the dependence of Y_1 on X_1 is inverse (i.e., larger values of X_1 correspond to lower values of Y_1) and nonlinear, since its CUSUNORO curve (**Fig. 4**) is always negative and its maximum absolute value is skewed from the median of X_1 (i.e., $CDF_1 = 0.5$). The critical value for X_1 is $x_{crit,1} = 0.43$ (vertical line in **Fig. 4**);
- the dependence of Y_1 on X_2 is direct and nonlinear, since its CUSUNORO curve (**Fig. 5**) is always positive and its maximum absolute value is skewed from the median of X_2 (i.e., $CDF_2 = 0.5$). The critical value for X_2 is $x_{crit,2} = 0.68$ (vertical line in **Fig. 5**);

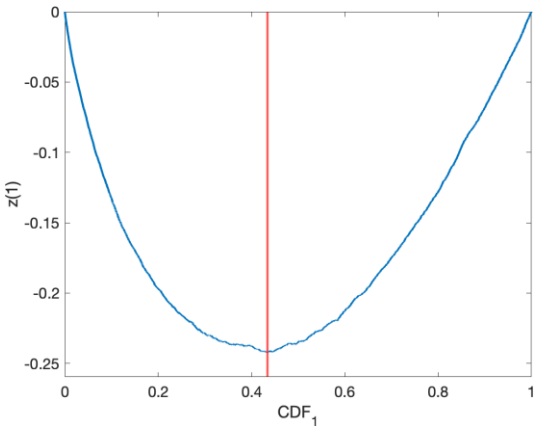

Fig. 4. CUSUNORO curve and critical value for X_1.

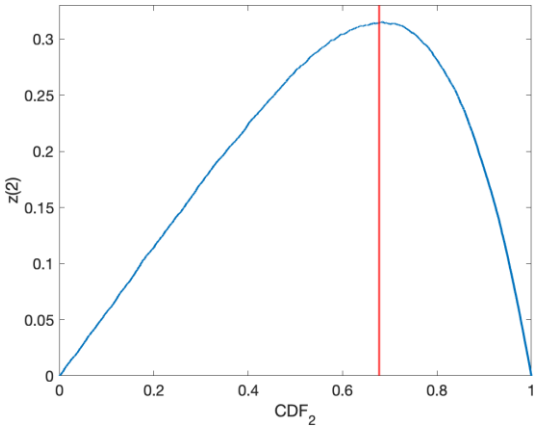

Fig. 5. CUSUNORO curve and critical value for X_2.

The critical values $x_{crit,1}$ and $x_{crit,2}$ provide insights on how the most relevant inputs should be constrained. To show this, PSM_Y is calculated considering different constraints on the minimum value of X_1 (due to the inverse dependency) and on the maximum value of X_2 (due to the direct dependency). This demonstrative analysis is feasible thanks to the very low computational cost of evaluating the analytic model of Eq. (15) and to the limited number of inputs. **Fig. 6** shows PSM_Y plotted against the minimum value of X_1 and the maximum value of X_2. By limiting X_1 and X_2 to their critical values (i.e., $X_1 \sim U(x_{crit,1}, 1)$ and $X_2 \sim U(0, x_{crit,2})$), the PSM is improved to $PSM_Y^* = 0.94$, which lies outside the region of rapid decrease in the PSM (i.e., the region characterized by closely spaced contour lines, where small changes in inputs cause significant changes in the PSM). It is important to note that for dependent inputs, it is necessary to truncate the support of the joint distribution to preserve dependencies, rather than truncating marginal supports independently. These insights can enable targeted and tailored design improvements, avoiding resorting to a computationally burdensome trial-and-error procedure, which would be unfeasible for the complex long running best-estimate SMR simulation models.

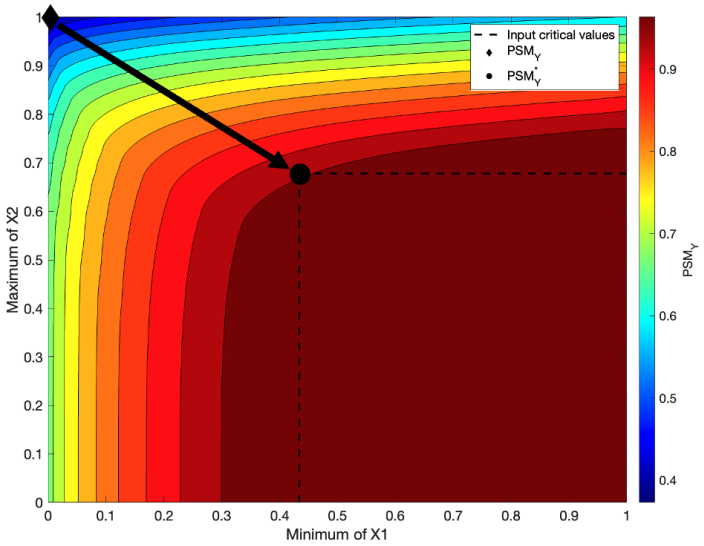

Fig. 6. PSM_Y as a function of the minimum value of X_1 and maximum value of X_2.

4. Application to the Safety Assessment of a Small Modular Reactor

In this Section, we apply the framework to analyze a case study that mimics a new concept reactor, which is still in the conceptual design phase. It is, thus, worth mentioning that the authors do not have access to detailed design information on the SMDFR and that the analysis has no marketing purpose. Subsection 4.1 presents the SMR design and the corresponding in-house developed simulation model. Subsection 4.2 presents the sensitivity analysis results and insights.

4.1. The SMR design and simulation

We consider a MU-NPP composed by $N = 4$ units of SMDFRs, the same as in [29]. A single unit of SMDFR is shown in **Fig. 7**. In this reactor design, the liquid fuel is a mixture of uranium tetrachloride and plutonium tetrachloride, which enters the core vessel at the bottom and spreads through a system of vertical tubes for the heat transfer before leaving the reactor from the top to enter the Pyrochemical Processing Unit (PPU). The liquid coolant is pure lead and enters the core vessel from the bottom to remove the heat from the fuel tubes by conduction before leaving the vessel from the top to enter the heat exchanger. We assume a 60-year design lifetime as in [49].

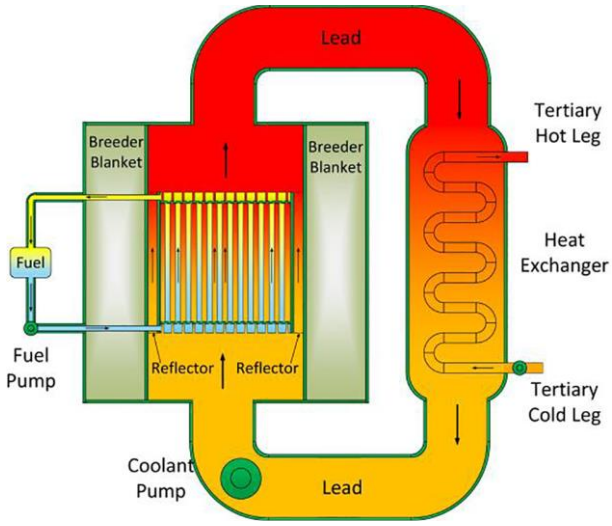

Fig. 7. Sketch of the SMDFR [50].

The design parameters of the SMDFRs are reported in **Tab. 1**.

Tab. 1. Design parameters of the SMDFR [28].

Parameter	**Value**
Core zone $D\ x\ H$ [m]	$0.95\ x\ 2.0$
Distribution zone $D\ x\ H$ [m]	$0.95\ x\ 0.2$
Collection zone $D\ x\ H$ [m]	$0.95\ x\ 0.2$
Height of the core [m]	2.4
Outer reflector diameter [m]	1.25
Tank $D\ x\ H$ [m]	$1.65\ x\ 3.4$
Number of fuel tubes	1027
Fuel pin pitch [m]	0.025
Outer/interior fuel tube diameter [m]	0.008/0.007
Outer/interior coolant tube diameter [m]	0.005/0.004
Mean linear power density [W/cm]	609
Fuel inlet temperature [K]	1300
Coolant inlet temperature [K]	973
Nominal peak cladding temperature [K], $T_{w,nom}$	1150
Fuel inlet velocity [m/s]	3
Coolant inlet velocity [m/s]	5

We assume that the system can be exposed to an earthquake with $PGA \in [0, 19.62] \frac{m}{s^2}$. The magnitude-frequency curve, whose CDF is used to calculate the failure probability of the system safety features to a random PGA, is taken from [51], without any specific reference to the case herein presented, and shown in **Fig. 8**. It is important to note that the the magnitude-frequency curve adopted

does not refer to any site-specific seismic design basis safety assessment, but it is used, without loss of generality, for the seismic hazard characterization of a hypothetical SMDFR site.

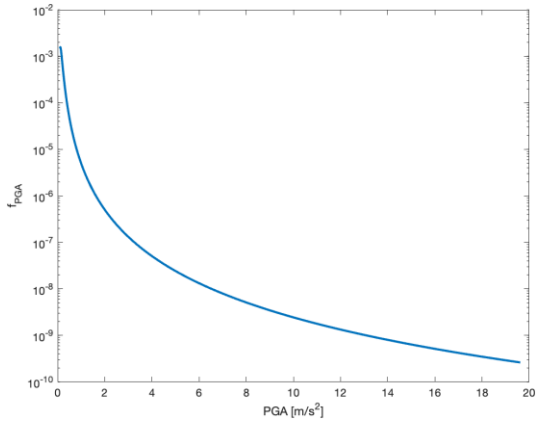

Fig. 8. Earthquake magnitude-frequency curve.

For illustrative purposes, we assume that, if the earthquake occurrence leads to a LOCA, the coolant leak flow rate $\dot{m}_{leak}$ is independent of the PGA value and the LOCA occurs at the outlet of the coolant pump. **Fig. 9** shows the leak flow rate as a function of time: the initial value is equal to the coolant flow rate in normal operating conditions, while the shape of the decrease of $\dot{m}_{leak}$ mimics the LOCA behavior in conventional Light Water Reactors (LWRs) [52]. This assumption is made because of the lack of specific data for LOCAs in SMDFRs.

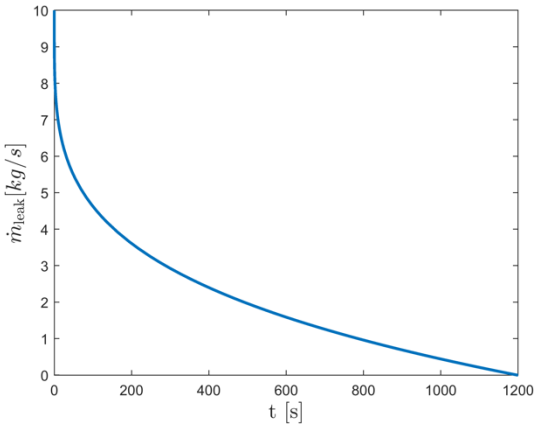

Fig. 9. LOCA leak flow rate.

To prevent the occurrence of a LOCA, the NPP is equipped with stainless steel CPs. Furthermore, for mitigation of the consequences of a LOCA, the NPP is equipped with four ACSs (one for each unit, with a modular piping system that allows sharing the flow among all units, while guaranteeing that each ACS can perform its safety function independently from the others, in line with the design criteria of the Nuclear Regulatory Commission (NRC) [53]), two EDGs (shared among all units, with each EDG being capable of providing power to all ACSs in case of LOP [54]), and four Melting Fuel

Plugs (MFPs) (one for each reactor), which are sections of molten salt designed to remain solid in normal operating conditions and to melt in case of a fuel temperature increase [29] (**Tab.2**).

Tab. 2. Safety features employed in the system.

Safety Feature	Classification	Description
Coolant Pipes (CP)	Passive, Preventive	Liquid lead containment
Auxiliary Cooling System (ACS)	Active, Mitigative	Auxiliary coolant delivery in case of LOCA
Emergency Diesel Generator (EDG)	Active, Mitigative	Independent source of power in case of LOP
Melting Fuel Plug (MFP)	Passive, Mitigative	Drains the fuel from the reactor in case of accident

The considered $s = 1,2, \dots, S$ safety features are actuated on demand with an uncertain response time t_s^r (**Tab. 3**, second column) and maintained each $\Delta t_{m,s}$ (**Tab. 3**, third column). The value of $\Delta t_{m,ACS}$ is assumed equal to that of an Auxiliary Feedwater System (AFS) of a typical LWR [55]; furthermore, $\Delta t_{m,CP}$ is necessarily synchronous to the periodic drainage of coolant and fuel from the reactor. No maintenance is considered for the MFP, which is assumed to be always available. Also, the maintenance is assumed to be perfect: safety features are restored to an As Good As New (AGAN) state upon maintenance.

Tab. 3. Safety features employed in the system.

Safety Feature	t_s^r	$\Delta t_{m,s}$
Coolant Pipes (CP)	$t_{r,CP} = 0$	$3\ y$
Auxiliary Cooling System (ACS)	$t_{r,ACS}$~[30,60] s [56]	$0.5\ y$ [55]
Emergency Diesel Generator (EDG)	$t_{r,EDG}$~[60,300] s [57]	$1.5\ y$ [58]
Melting Fuel Plug (MFP)	$t_{r,MFP} = 1200\ s$ ([29], [59], [60])	-

The probability of failure of the safety features is composed of the probability of failure due to internal causes and that due to external hazards [30]. The degradation of the safety features is accounted for, as in previous works ([30], [61]), by embedding Physics-of-Failure (PoF) models into the safety features fragility models which, ultimately, provides fragility surfaces as functions of both the hazard magnitude and the safety feature age.

A one-dimensional lumped parameter model that simulates safe and accidental conditions transients that might occur in the system is used for the risk assessment ([28], [62]). The model inputs are reported in **Tab. 4** with their respective probability distributions. The selected inputs for the sensitivity analysis are those related with the safety features of the reactors, in line with that done in [30].

Tab. 4. Model inputs probability distributions.

Input	Description	Probability distribution
PGA	Earthquake Peak Ground Acceleration $\left[\frac{m}{s^2}\right]$	$PGA \sim Frechet(2.31,\ 0.133)$ [51]
Age	Age of the system $[y]$	$Age \sim U(0,60)$
$d_{in,CP}$	Initial depth of CP corrosion defect $[mm]$	$d_{in,C} \sim N(1.59,\ 0.619)$ [63]
$d_{in,ACS}$	Initial depth of ACS corrosion defect $[mm]$	$d_{in,ACS} \sim N(1.59,\ 0.619)$ [63]
$d_{in,EDG}^{C}$	Initial depth of EDG corrosion defect $[mm]$	$d_{in,EDG}^{C} \sim N(1.59,\ 0.619)$ [63]
t_{ACS}^{r}	Response time of ACS $[s]$	$t_{ACS}^{r} \sim U(30,60)$ [56]
t_{EDG}^{r}	Response time of EDG $[s]$	$t_{EDG}^{r} \sim U(60,300)$ [57]
t_{ACS}^{f}	Failure time of ACS $[s]$	$t_{ACS} \sim U(15, t_{sim})$, with mean value $t_{ACS}^{mean} = 607.5\ s$
t_{EDG}^{f}	Failure time of EDG $[s]$	$t_{EDG} \sim U(15, t_{sim})$, with mean value $t_{EDG}^{mean} = 607.5\ s$

The dynamic model [28] considers a time horizon $T_s = 1200\ s$, which is the time allowed to confirm that the drainage of the fuel from the reactor core through the MFP is successful ([29], [59], [60]) and, thus, the accident is successfully mitigated. The model output is the peak cladding temperature $T_{w,n}(t)$ of each *n-th* reactor unit, since it is considered as the safety parameter of interest, and the threshold not to be exceeded during the accident is $T_{w,fail} = 1244\ K$. This is set by assuming that T_w must never exceed the thermal stress inducing a loss of structural integrity of the fuel pipes: in practice, the thermal stress on the fuel pipes is given by:

$$\sigma_{th} = E\gamma(T)\Delta T \tag{16}$$

where $E = 207\ GPa$ is the Young's Modulus of Nickel 201, which is the candidate material for Molten Salt Reactors (MSRs) [64], $\gamma(T)$ is the temperature-dependent coefficient of thermal expansion (estimated interpolating the data in [65]) and ΔT is the temperature change of the fuel pipes. By setting $\sigma_{th} = \sigma_{UTS} = 345\ MPa$, which is the ultimate tensile strength of the pipe, it is possible to calculate the temperature change that leads to a loss of structural integrity (i.e., $\Delta T_{fail} = 94\ °C$ and $T_{w,fail} = T_{w,nom} + \Delta T_{fail} = 1244\ K$). In **Fig. 10**, two example transients are shown.

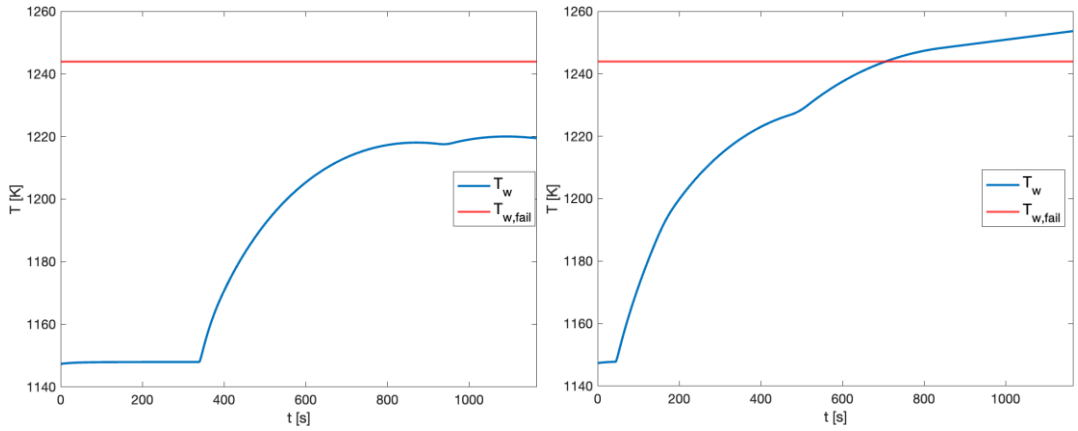

Fig. 10. Example transients of $T_{w,1}$: on the left a safe transient and on the right a failed transient; the solid straight line indicates the failure threshold.

4.2. Sensitivity Analysis: Results and Insights

The GSA framework presented in Section 3 is applied to the case study of Section 4.1. The available data consists of $N_{sim} = 10^4$ simulations of accidental scenarios (i.e., scenarios in which at least one of the reactors experiences a LOCA), generated in approximately $28h$ on a commercially available laptop with an AMD Ryzen 5 PRO 4650U processor. The total number of simulations (including those without a LOCA) is $N_{sim}^{total} = 10^7$. The median PGA for scenarios with only one LOCA is $PGA_{single}^{median} = 5.25 \frac{m}{s^2}$, while for scenarios with multiple LOCAs it is $PGA_{multiple}^{median} = 14.27 \frac{m}{s^2}$. The GSA is conducted considering the input parameters of **Tab. 4** and the output of interest is the maximum value of $T_{w,n}$ reached during the accidental scenario (i.e., $T_{w,max,n}$), for each *n-th* reactor unit.

4.2.1. Parameter prioritization

Fig. 11 shows the results of the parameter prioritization, where a dummy input (i.e., a fictitious input with no influence on the output) is added to facilitate the relative identification of uninfluential input parameters.

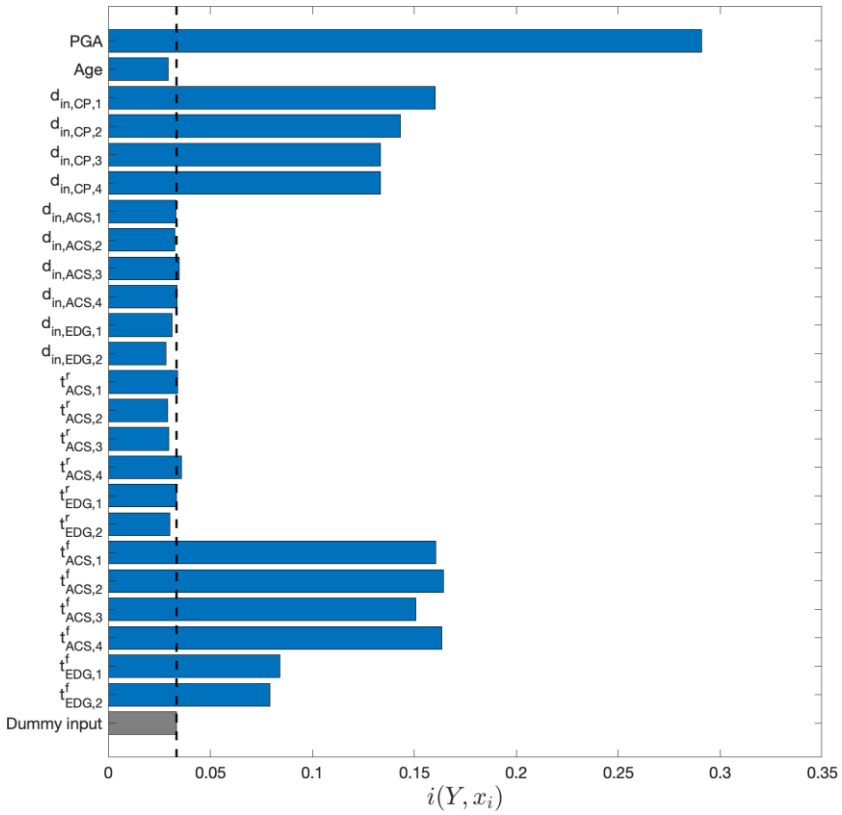

Fig. 11. Parameter prioritization results.

The following considerations are made based on the parameter prioritization results:

- the PGA is the most important input; therefore, improvements should focus on anti-seismic measures;
- the failure times of the mitigative safety features (i.e., t^f_{ACS} and t^f_{EDG}) are more important that their response times (i.e., t^r_{ACS} and t^r_{EDG}); therefore, it is more beneficial to focus on improving the reliability of those safety features rather than their response speed;
- the initial depth of the corrosion defect of the CPs (i.e., $d_{in,CP}$) is among the most important inputs; therefore, an improvement to the CP resistance to corrosion can be beneficial for the system safety;
- the age of the system does not impact $T_{w,max}$ significantly; this is due to the "perfect" (AGAN) maintenance adopted for the system, which diminishes the impact of aging and degradation on the system safety.

Finally, we identify the most important inputs considering the hypothesis of perfect maintenance as the most realistic, leading to the identification of PGA, $d_{in,CP,n}$ and $t^f_{ACS,n}$ as the most important inputs.

To investigate the influence of the assumption of perfect maintenance, parameter prioritization has been reconsidered based on a set of $N_{sim,2} = 10^3$ simulated accidental scenarios with imperfect maintenance interventions (degradation of safety features only reduced and not completely eliminated) according to the same schedule of **Tab. 3**. The imperfect maintenance model adopted is the one described in ([66], [67]), based on the calculation of the effective age of the maintained component:

$$\tau_E^q = \tau_E^{q-1} + \alpha \Delta t_m \tag{17}$$

where τ_E^q is the effective age immediately after the *q-th* maintenance intervention, α is the effectiveness of the maintenance intervention ($\alpha = 0$ represents perfect maintenance, i.e. AGAN; $\alpha = 1$ represents completely ineffective maintenance, i.e. As Good As Old (AGAO)) and Δt_m is the time between two successive maintenance interventions. To show the impact of imperfect maintenance, we assume $\alpha = 0.1$.

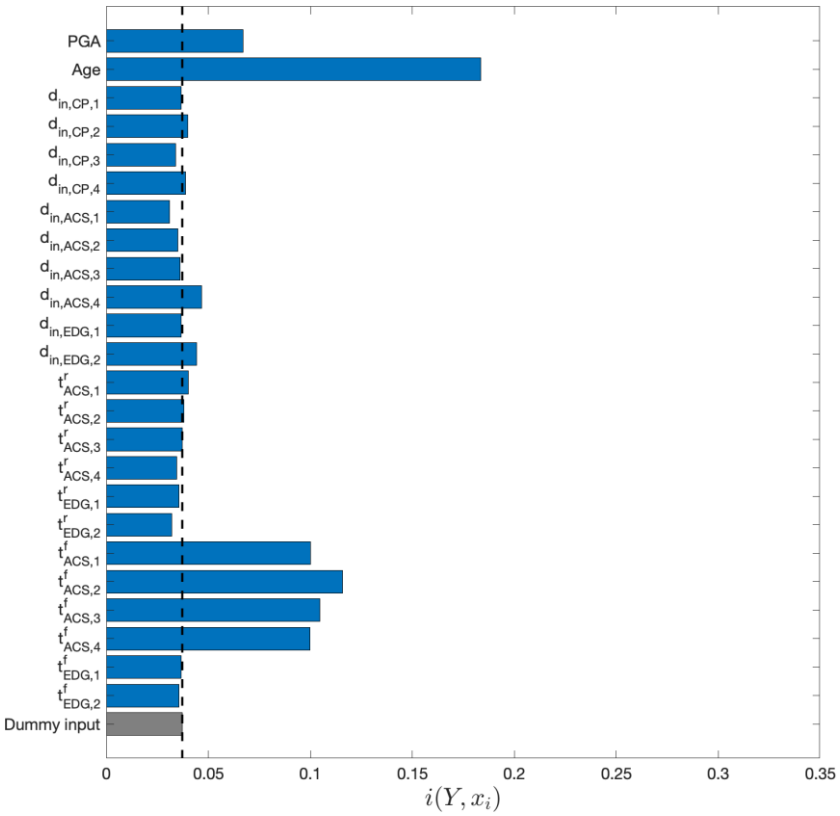

Fig. 12. Parameter prioritization results considering imperfect maintenance.

As shown in **Fig. 12**, age becomes the most important input when imperfect maintenance is considered. In this case, an improvement to the maintenance strategy should be taken into account to reduce the impact of liquid lead corrosion ([68], [69]).

Lastly, a univariate parameter prioritization (i.e., considering $T_{w,max}$ of a single reactor unit at a time) has been performed based on the N_{sim} simulated accidental scenarios obtained with perfect maintenance. The prioritization is calculated using the squared 2-Wasserstein distance [25] and the results are compared with those of the multivariate parameter prioritization of **Fig. 11**.

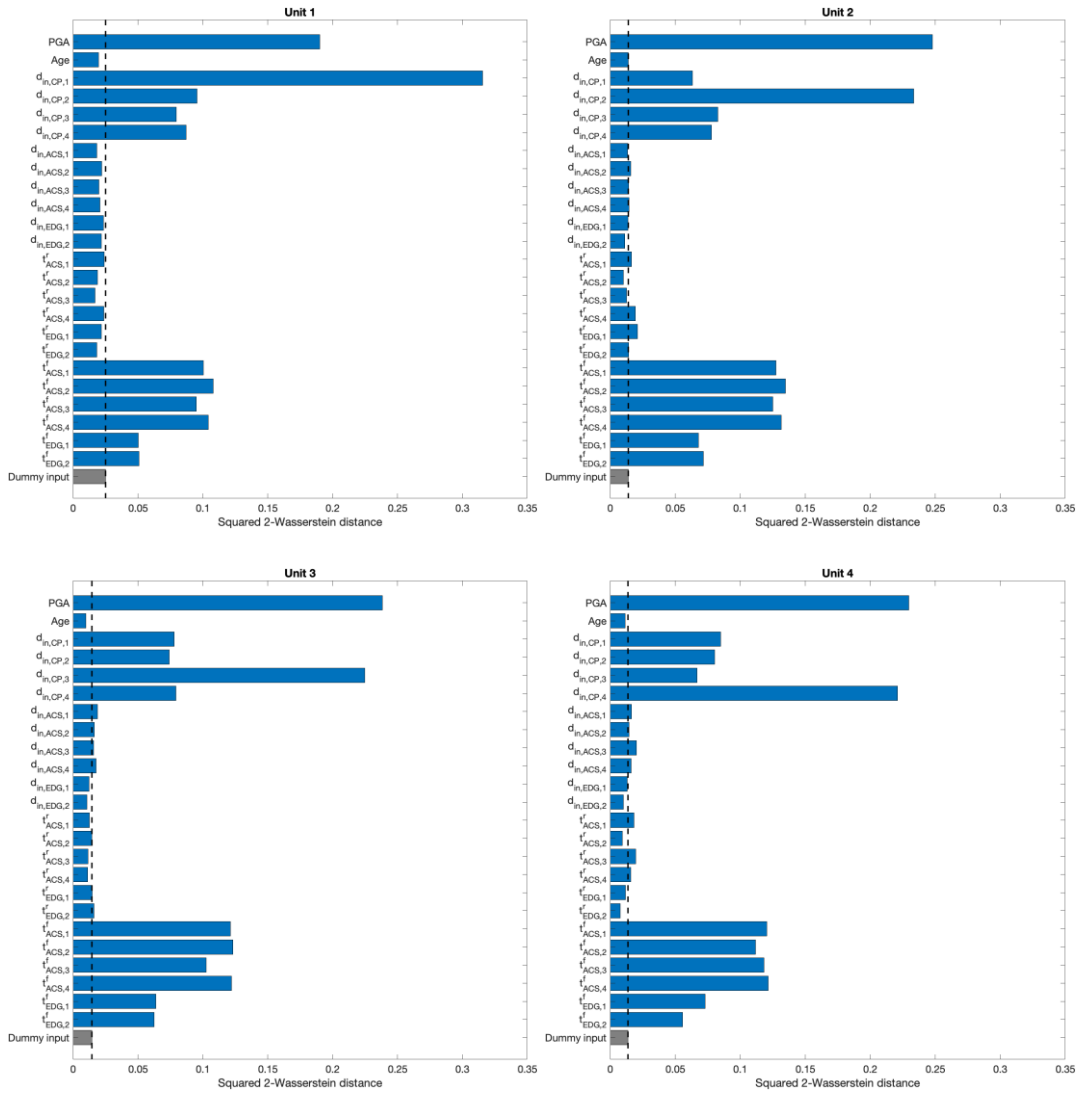

Fig. 13. Univariate parameter prioritization results for unit 1 (top-left), unit 2 (top-right), unit 3 (bottom-left) and unit 4 (bottom-right).

As shown in **Fig. 13**, the results of the univariate analysis assign, for each *n-th* unit, a larger importance to $d_{in,CP,n}$, that, for unit $n = 1$, seems to be more important than PGA. This does not occur for all units because of the fluctuations of the estimates induced by the limited number of simulations available in the dataset. It is also worth noting that $d_{in,CP,n}$ has a non-negligible impact on the other SMR units. This is due to the fact that the units share the ACSs: a large initial depth of the CP corrosion defect increases the probability of a LOCA in the *n-th* unit; if LOCAs occur

simultaneously in multiple units, the coolant mass flow provided by the ACSs must be shared, with a reduced mitigative effect.

4.2.2. Critical input segmentation

The critical input segmentation of PGA, $d_{in,CP,n}$ and $t^f_{ACS,n}$ is performed to identify the critical input values and provide guidelines for design improvement. For the sake of brevity, in what follows we consider only the analysis and results of the first reactor unit ($n = 1$), whose CUSUNORO curve is shown in **Fig. 14**.

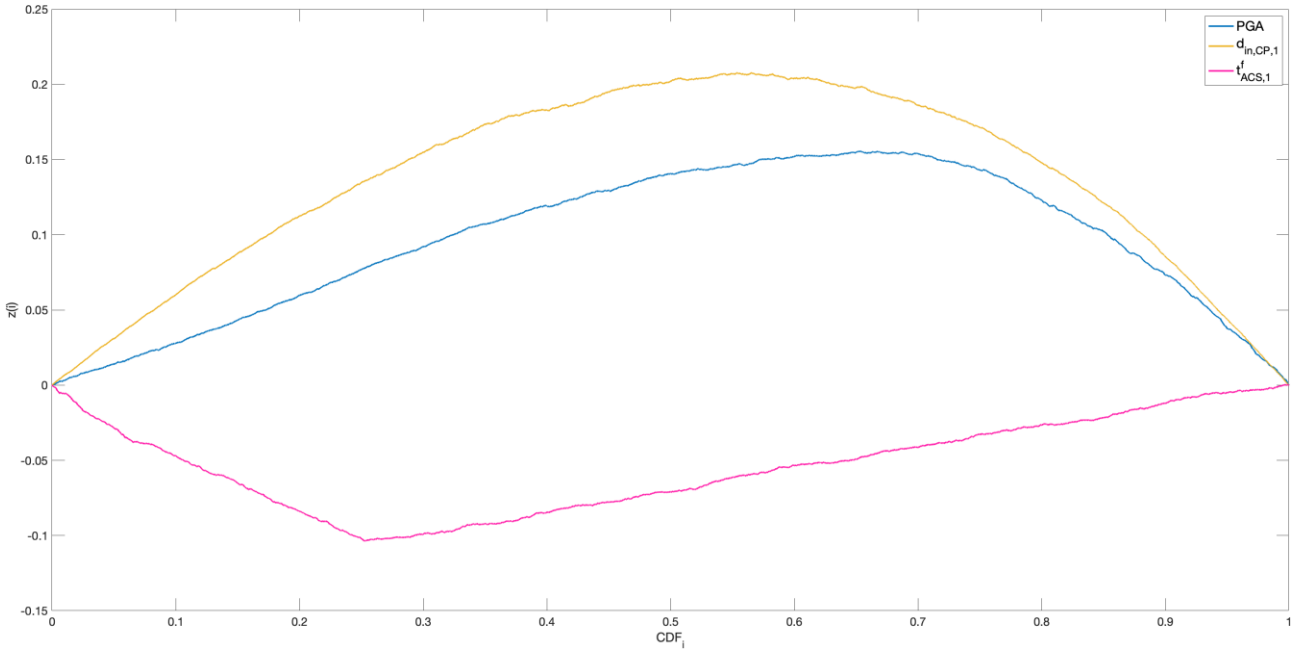

Fig. 14. CUSUNORO results for PGA, $d_{in,CP,1}$ and $t^f_{ACS,1}$ considering $T_{w,max,1}$.

The following considerations about the most important inputs emerge:

- $T_{w,max,1}$ has a direct and (almost) linear dependence on $d_{in,CP,1}$, since the maximum value of the CUSUNORO curve is (almost) centered on the median of $d_{in,CP,1}$, preventing the identification of a critical value for $d_{in,CP,1}$; nevertheless, given the importance of $d_{in,CP,1}$ (**Fig. 11**), design improvements should still focus on the improvement of the CP resistance to corrosion by employing, for example, a low alloyed Fe-10Cr-4Al steel [70];
- $T_{w,max,1}$ has a nonlinear dependence on the PGA (direct dependence) and the failure time of ACS (inverse dependence), since the maximum value of the corresponding CUSUNORO curves is significantly skewed from the median of the respective inputs; the critical value for the failure time of ACS is $t^f_{ACS,1,crit} = 317\ s$ (**Fig. 15**) and the critical value for the PGA is $PGA_{crit} = 11.61\,\frac{m}{s^2}$ (**Fig. 16**). While not directly linked with design acceptance criteria, the

critical values identify regions of large output sensitivity to input variations, which may suggest increased risk sensitivity if operating in those regions.

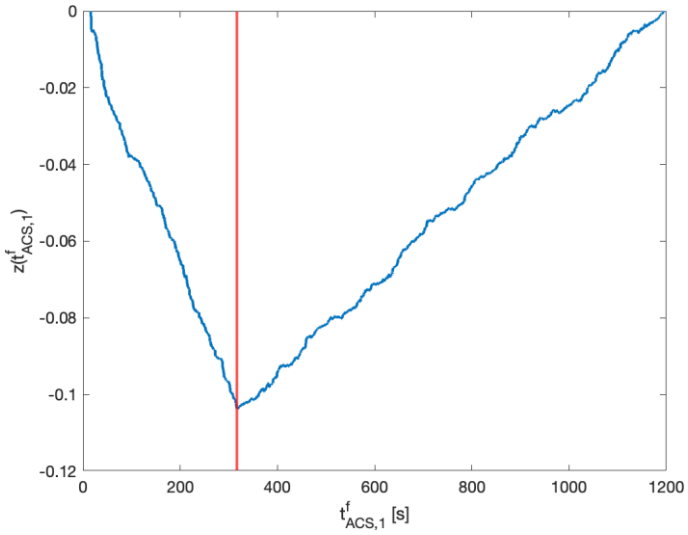

Fig. 15. Critical value of ACS failure time.

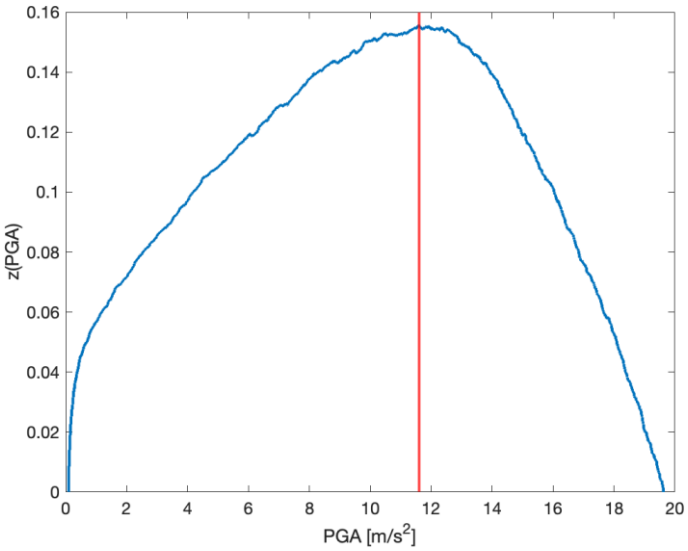

Fig. 16. Critical value of PGA.

Possible design improvements could, then, be:

- reducing the probability of early failures of ACS, to avoid the region in which $t^f_{ACS,1} \leq t^f_{ACS,1,crit}$ and increase the distance from the CR; this can be achieved by increasing the ACS seismic resilience, as earthquake-induced failures tend to occur at the beginning of the accidental scenario, whereas failures due to random internal causes are uniformly distributed in time;
- reducing the earthquake impact on the NPP, effectively shifting the CR to larger PGA values.

Since it is obviously not possible to control the earthquake magnitude to avoid the region in which $PGA \geq PGA_{crit}$, in practice both objectives can be achieved by improving the NPP overall seismic resilience. As an example, let us consider the installation of viscous dampers to the NPP buildings. To evaluate the effect of damping on the fragility of a concrete building, we first define the fragility as in [71]:

$$F(PGA) = \phi\left(\frac{1}{\beta}\ln\left(\frac{PGA}{\mu}\right)\right) \tag{18}$$

where ϕ is the standard normal cumulative distribution function, μ is the median seismic capacity and β is the standard deviation of the logarithmic median capacity. By installing a viscous damper with damping coefficient D, the median capacity of the building increases as follows [71]:

$$\mu^*(D) = \mu \cdot \frac{(73.048 \cdot \ln(D) - 112)}{100} \tag{19}$$

To find a suitable damping coefficient, we use the distribution shown in **Fig. 8** to estimate the PGA value for the design basis earthquake (SL-2 level), defined as the ground motion with an annual frequency of exceedance of 10^{-4}. To account for beyond design basis conditions, we apply a conservative amplification factor of 1.4 to this value, leading to $PGA_{BDBE} = 18\frac{m}{s^2}$ [72]. Finally, the damping coefficient D is found as the one that leads to $P^*_{F,s}(PGA_{BDBE}) \leq P_{F,s}(PGA_{crit})$ for all $s = 1,2,\dots,S$ safety features, where $P_{F,s}$ is the failure probability of the *s-th* safety feature considering the original SMR design and $P^*_{F,s}$ is the failure probability of the *s-th* safety feature considering the improved SMR design, leading to $D \geq 42\%$. Note that, given the lack of facility-specific models linking the seismic capacity to the damping coefficient, the model in Eq. (19), developed for concrete buildings, has been adopted to illustrate the proposed framework, and the results are not intended to serve as an actual design basis for nuclear facilities.

4.2.3. Implementation of the GSA-driven design improvements

To summarize, the following improvements are identified by the GSA framework:

- improvement of the CP resistance to corrosion by employing, for example, a low alloyed Fe-10Cr-4Al steel [70];
- improvement of the NPP seismic reliability by installing viscous dampers with a damping coefficient $D \geq 42\%$;

While a conventional full-scope Probabilistic Safety Assessment (PSA) would identify the need for improved seismic resilience in general terms, the proposed GSA framework provides additional, more targeted design insights. For example, the parameter prioritization results specifically highlight that

improving the failure times of the ACSs is more beneficial than reducing their response times, suggesting a focus on reliability enhancements and/or specific maintenance strategies rather than responsiveness. The analysis also shows the significant role of corrosion defect depth in the CP, pointing to a different material as a targeted design improvement. Additionally, critical input segmentation provides quantitative input thresholds that define regions of increased system sensitivity, which can guide setting design targets, such as the required damping coefficient. Overall, these insights can help the decision-maker prioritize design improvements to comply with regulations.

To show the impact of implementing the identified design improvements on the system safety, we perform $N^*_{sim} = 10^4$ simulations of accidental scenarios with the same simulation model, accounting for the above improvements in system design. The comparison between the results before (**Fig. 17**) and after (**Fig. 18**) the design improvements lead to the following considerations:

- the number of system failures (i.e., the filled red dots) is significantly reduced, and failures occur at larger PGA values;
- the number of ACS failures is significantly reduced (note that when $t^f_{ACS,1} = 1200\ s$, ACS is not failed);

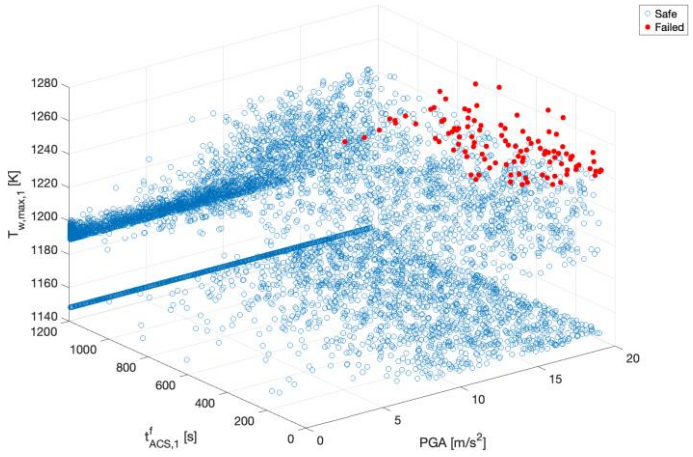

Fig. 17. $T_{w,max,1}$ as a function of PGA and $t^f_{ACS,1}$ with the original design.

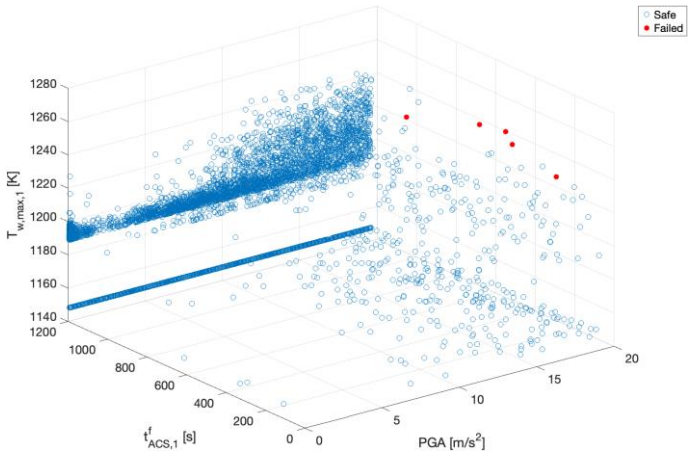

Fig. 18. $T_{w,max,1}$ as a function of PGA and $t^f_{ACS,1}$ with the improved design.

Consequently, the CR obtained with the improved design is shifted to larger PGA values and is significantly smaller with respect to the CR obtained with the original design, as shown in **Fig. 19**, resulting in a safer operation of the reactor.

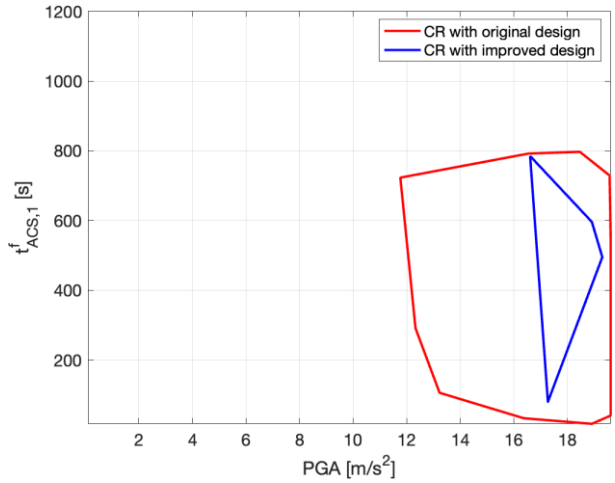

Fig. 19. CR boundary with original and improved design.

Finally, the results are also compared in terms of $PSM_{T_{w,max,1}}$ (with $\gamma = 95$) and probability of failure of the first reactor (i.e., $F_{P,1}$). As shown in **Fig. 20** and **Fig. 21**, the improved design achieves a significantly larger PSM (~53% increase) and a significantly lower failure probability (~95% decrease), showing the benefits of implementing the identified design improvements.

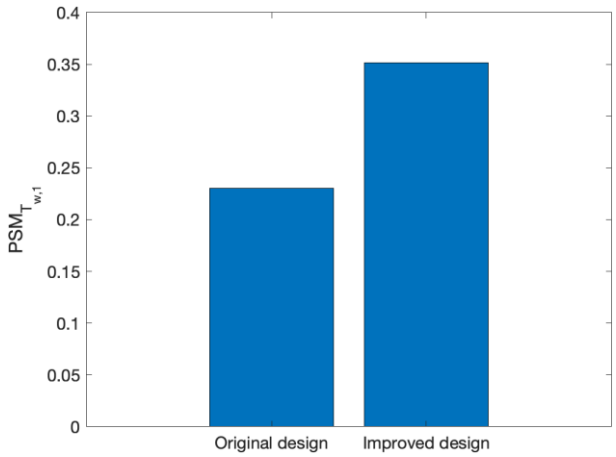

Fig. 20. $PSM_{T_{w,max,1}}$ comparison between original and improved design.

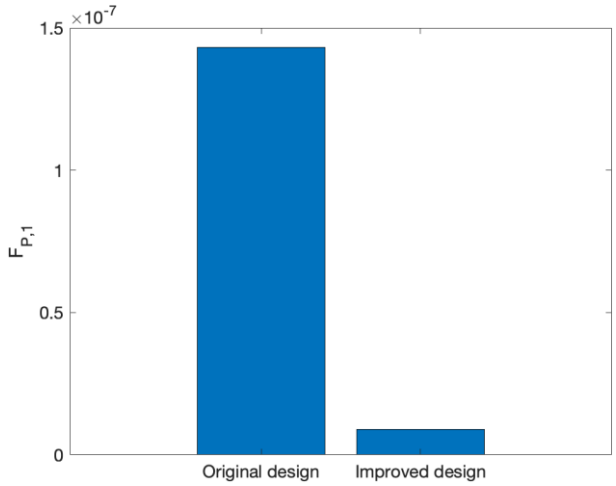

Fig. 21. $F_{P,1}$ comparison between original and improved design.

4.3. Discussion

The proposed framework can provide valuable insights to assist in the modeling phase of an SMR design, under the following constraints:

- the validity of the sensitivity analysis results is inherently dependent on the fidelity of the simulation model: if the model does not satisfy the accuracy and predictiveness requirements necessary for its intended use in safety analysis and design decision-making [73], the sensitivity analysis results may be misleading;
- the estimation accuracy of global sensitivity measures increases with the sample size, and the natural recommendation is to use the largest size allowed by computational budget. In our case, the estimation design is given data and allows the analyst to devote the entire budget to one Monte Carlo uncertainty quantification, thus increasing the sample size as much as possible. However, as the literature widely documents, uncertainty quantification becomes problematic for models with long running times. In these cases, the literature suggests

alternative approaches. On the one hand, one can reduce computational burden by approximating time-consuming calculations in the original simulators by artificial intelligence tools or model emulators ([74], [75]). On the other hand, one can use exploration-exploitation strategies and mix high- and low-fidelity simulations [76]. Alternatively, one can plan the experiments in two steps, with first a careful selection of the points of the input space through a space-filling design [77], and then fitting a metamodel to propagate uncertainty, also preceding the analysis with a screening exercise ([17], [78]). If the metamodel fit is accurate, several runs can be obtained in a short amount of time. The utilization of these strategies to reduce computational burden is a field in constant evolution in the modeling of technological systems, recently accelerated by the rapid progress in artificial intelligence techniques.

5. Conclusions

We have proposed a novel GSA framework to assist in the modeling phase of an SMR design. First, the inputs most impacting the safety of the SMR are identified using OT-based GSA indices. Then, critical parameters segmentation is performed with CUSUNORO to identify the critical input values and provide guidelines for the design improvements aimed at keeping the SMR away from the CR.

The framework has been applied to a case study concerning an SMR installation composed by four SMDFRs. The results of the OT-based parameter prioritization identify the PGA, the corrosion of CP and the failure time of ACS as the most important inputs, and the results of the parameters segmentation provide guidelines on the critical values of these inputs. Based on these findings, potential improvements to the system design are the improvement of the CP resistance to corrosion and the installation of viscous dampers to improve the system seismic reliability.

Future work might investigate the scalability of the proposed framework to a real high-dimensional problem, whose model entails a large number of correlated inputs and many outputs.

References

[1] Z. Liu and J. Fan, "Technology readiness assessment of Small Modular Reactor (SMR) designs," *Progress in Nuclear Energy*, vol. 70, pp. 20–28, Jan. 2014, doi: 10.1016/J.PNUCENE.2013.07.005.

[2] J. Vujić, R. M. Bergmann, R. Škoda, and M. Miletić, "Small modular reactors: Simpler, safer, cheaper?," *Energy*, vol. 45, no. 1, 2012, doi: 10.1016/j.energy.2012.01.078.

[3] International Atomic Energy Agency (IAEA), "SSR-2/1 (Rev. 1): Safety of Nuclear Power Plants: Design," 2016.

[4] L. Puppo, N. Pedroni, F. Di Maio, A. Bersano, C. Bertani, and E. Zio, "A Framework based on Finite Mixture Models and Adaptive Kriging for Characterizing Non-Smooth and Multimodal Failure Regions in a Nuclear Passive Safety System," *Reliab Eng Syst Saf*, vol. 216, p. 107963, Dec. 2021, doi: 10.1016/J.RESS.2021.107963.

[5] H. A. Gabbar and O. L. A. Esteves, "Real-Time Simulation of a Small Modular Reactor in-the-Loop within Nuclear-Renewable Hybrid Energy Systems," *Energies (Basel)*, vol. 15, no. 18, 2022, doi: 10.3390/en15186588.

[6] B. Poudel, K. Joshi, and R. Gokaraju, "A Dynamic Model of Small Modular Reactor Based Nuclear Plant for Power System Studies," *IEEE Transactions on Energy Conversion*, vol. 35, no. 2, 2020, doi: 10.1109/TEC.2019.2956707.

[7] J. Fang *et al.*, "Feasibility of full-core pin resolved CFD simulations of small modular reactor with momentum sources," *Nuclear Engineering and Design*, vol. 378, 2021, doi: 10.1016/j.nucengdes.2021.111143.

[8] K. Podila *et al.*, "Demonstration of a coupled computational fluid dynamics approach for modelling non-water cooled small modular reactors," *Ann Nucl Energy*, vol. 159, 2021, doi: 10.1016/j.anucene.2021.108346.

[9] J. Hamel, M. Li, and S. Azarm, "Design improvement by sensitivity analysis under interval uncertainty using multi-objective optimization," *Journal of Mechanical Design*, vol. 132, no. 8, 2010, doi: 10.1115/1.4002139.

[10] E. Borgonovo and G. E. Apostolakis, "A new importance measure for risk-informed decision making," *Reliab Eng Syst Saf*, vol. 72, no. 2, 2001, doi: 10.1016/S0951-8320(00)00108-3.

[11] J. C. Helton, “Uncertainty and sensitivity analysis techniques for use in performance assessment for radioactive waste disposal,” *Reliab Eng Syst Saf*, vol. 42, no. 2–3, 1993, doi: 10.1016/0951-8320(93)90097-I.

[12] A. Saltelli, K. Chan, and E. Scott, *Sensitivity Analysis*. Chichester: John Wiley & Sons, 2000.

[13] M. P. Butler, P. M. Reed, K. Fisher-Vanden, K. Keller, and T. Wagener, “Identifying parametric controls and dependencies in integrated assessment models using global sensitivity analysis,” *Environmental Modelling and Software*, vol. 59, 2014, doi: 10.1016/j.envsoft.2014.05.001.

[14] M. Fonoberova, V. A. Fonoberov, and I. Mezić, “Global sensitivity/uncertainty analysis for agent-based models,” *Reliab Eng Syst Saf*, vol. 118, 2013, doi: 10.1016/j.ress.2013.04.004.

[15] T. A. Mara and S. Tarantola, “Application of global sensitivity analysis of model output to building thermal simulations,” *Build Simul*, vol. 1, no. 4, 2008, doi: 10.1007/s12273-008-8129-5.

[16] P. Kumar, B. Sanderse, K. Boorsma, and M. Caboni, “Global sensitivity analysis of model uncertainty in aeroelastic wind turbine models,” in *Journal of Physics: Conference Series*, 2020. doi: 10.1088/1742-6596/1618/4/042034.

[17] E. Cervi, X. Lu, A. Cammi, F. Di Maio, and E. Zio, “Sensitivity-Analysis-Driven Surrogate Model for Molten Salt Reactors Control,” *Journal of Nuclear Engineering*, vol. 3, no. 4, 2022, doi: 10.3390/jne3040016.

[18] F. Di Maio, T. Matteo Coscia, N. Pedroni, A. Bersano, F. Mascari, and E. Zio, “Global Sensitivity Analysis for Segmented Inverse Uncertainty Quantification in the Safety Analysis of Nuclear Power Plants,” *Ann Nucl Energy*, vol. 208, p. 110791, Dec. 2024, doi: 10.1016/J.ANUCENE.2024.110791.

[19] X. Zheng, H. Itoh, K. Kawaguchi, H. Tamaki, and Y. Maruyama, “Application of Bayesian nonparametric models to the uncertainty and sensitivity analysis of source term in a BWR severe accident,” *Reliab Eng Syst Saf*, vol. 138, pp. 253–262, Jun. 2015, doi: 10.1016/J.RESS.2015.02.004.

[20] Q. Xiong *et al.*, “Global sensitivity analysis for nuclear reactor LBLOCA with time-dependent outputs,” *Reliab Eng Syst Saf*, vol. 221, 2022, doi: 10.1016/j.ress.2022.108337.

[21] M. Pusa, “Perturbation-theory-based sensitivity and uncertainty analysis with CASMO-4,” *Science and Technology of Nuclear Installations*, vol. 2012, 2012, doi: 10.1155/2012/157029.

[22] R. P. Martin and A. Petruzzi, “Progress in international best estimate plus uncertainty analysis methodologies,” *Nuclear Engineering and Design*, vol. 374, 2021, doi: 10.1016/j.nucengdes.2020.111033.

[23] T. Zhou, M. Modarres, and E. L. Droguett, “A review of multi-unit nuclear power plant probabilistic risk assessment research,” in *International Conference on Nuclear Engineering, Proceedings, ICONE*, 2018. doi: 10.1115/ICONE26-81130.

[24] T. D. Le Duy and D. Vasseur, “A practical methodology for modeling and estimation of common cause failure parameters in multi-unit nuclear PSA model,” *Reliab Eng Syst Saf*, vol. 170, pp. 159–174, Feb. 2018, doi: 10.1016/J.RESS.2017.10.018.

[25] E. Borgonovo, A. Figalli, E. Plischke, and G. Savaré, “Global Sensitivity Analysis via Optimal Transport,” *Manage Sci*, Aug. 2024, doi: 10.1287/mnsc.2023.01796.

[26] E. Plischke, “An adaptive correlation ratio method using the cumulative sum of the reordered output,” in *Reliability Engineering and System Safety*, 2012. doi: 10.1016/j.ress.2011.12.007.

[27] E. Plischke, E. Borgonovo, and C. L. Smith, “Global sensitivity measures from given data,” *Eur J Oper Res*, vol. 226, no. 3, pp. 536–550, May 2013, doi: 10.1016/J.EJOR.2012.11.047.

[28] C. Liu, R. Luo, and R. Macián-Juan, “A new uncertainty-based control scheme of the small modular dual fluid reactor and its optimization,” *Energies (Basel)*, vol. 14, no. 20, Oct. 2021, doi: 10.3390/en14206708.

[29] A. Huke, G. Ruprecht, D. Weißbach, S. Gottlieb, A. Hussein, and K. Czerski, “The Dual Fluid Reactor - A novel concept for a fast nuclear reactor of high efficiency,” *Ann Nucl Energy*, vol. 80, pp. 225–235, 2015, doi: 10.1016/j.anucene.2015.02.016.

[30] S. Marchetti, F. Di Maio, and E. Zio, “An Integrated Deterministic and Probabilistic Safety Assessment of Multi-Unit Small Modular Reactors considering the degradation of shared safety barriers,” *Nuclear Science and Engineering*, 2025, doi: https://doi.org/10.1080/00295639.2025.2515349.

[31] J. C. Helton, “Risk, uncertainty in risk, and the EPA release limits for radioactive waste disposal,” *Nucl Technol*, vol. 101, no. 1, 1993, doi: 10.13182/NT93-A34765.

[32] N. A. Eisenberg and B. Sagar, “Importance measures for nuclear waste repositories,” *Reliab Eng Syst Saf*, vol. 70, no. 3, 2000, doi: 10.1016/S0951-8320(00)00050-8.

[33] T. Ikonen, “Comparison of global sensitivity analysis methods - Application to fuel behavior modeling,” *Nuclear Engineering and Design*, vol. 297, 2016, doi: 10.1016/j.nucengdes.2015.11.025.

[34] E. Borgonovo, G. B. Hazen, and E. Plischke, “A Common Rationale for Global Sensitivity Measures and Their Estimation,” *Risk Analysis*, vol. 36, no. 10, 2016, doi: 10.1111/risa.12555.

[35] R. L. Iman and S. C. Hora, “A Robust Measure of Uncertainty Importance for Use in Fault Tree System Analysis,” *Risk Analysis*, vol. 10, no. 3, 1990, doi: 10.1111/j.1539-6924.1990.tb00523.x.

[36] Y. Chen, T. T. Georgiou, and M. Pavon, “Stochastic control liaisons: Richard Sinkhorn meets gaspard monge on a schrödinger bridge,” 2021. doi: 10.1137/20M1339982.

[37] C. Villani, “Optimal Transport Old and New,” *Media*, vol. 338, 2007.

[38] G. Peyré and M. Cuturi, “Computational optimal transport,” *Foundations and Trends in Machine Learning*, vol. 11, no. 5–6, 2019, doi: 10.1561/2200000073.

[39] C. R. Givens and R. M. Shortt, “A class of Wasserstein metrics for probability distributions.,” *Michigan Mathematical Journal*, vol. 31, no. 2, 2002, doi: 10.1307/mmj/1029003026.

[40] M. Gelbrich, “On a Formula for the L2 Wasserstein Metric between Measures on Euclidean and Hilbert Spaces,” *Mathematische Nachrichten*, vol. 147, no. 1, 1990, doi: 10.1002/mana.19901470121.

[41] S. Chatterjee, “A New Coefficient of Correlation,” *J Am Stat Assoc*, vol. 116, no. 536, 2021, doi: 10.1080/01621459.2020.1758115.

[42] T. Ishlg-Ami and T. Homma, “An importance quantification technique in uncertainty analysis for computer models,” in *Proceedings of ISUMA 1990 - 1st International Symposium on Uncertainty Modeling and Analysis*, 1990. doi: 10.1109/ISUMA.1990.151285.

[43] S. S. Vallender, “Calculation of the Wasserstein Distance Between Probability Distributions on the Line,” *Theory of Probability & Its Applications*, vol. 18, no. 4, 1974, doi: 10.1137/1118101.

[44] D. G. Luenberger and Y. Ye, *Linear and nonlinear programming (4th ed.)*. Springer, 2021.

[45] H. W. Kuhn, “Variants of the hungarian method for assignment problems,” *Naval Research Logistics Quarterly*, vol. 3, no. 4, 1956, doi: 10.1002/nav.3800030404.

[46] M. Cuturi, “Sinkhorn distances: Lightspeed computation of optimal transport,” in *Advances in Neural Information Processing Systems*, 2013.

[47] F. Di Maio *et al.*, “Accounting for Safety Barriers Degradation in the Risk Assessment of Oil and Gas Systems by Multistate Bayesian Networks,” *Reliab Eng Syst Saf*, vol. 216, p. 107943, Dec. 2021, doi: 10.1016/J.RESS.2021.107943.

[48] F. Di Maio, A. Rai, and E. Zio, “A dynamic probabilistic safety margin characterization approach in support of Integrated Deterministic and Probabilistic Safety Analysis,” *Reliab Eng Syst Saf*, vol. 145, 2016, doi: 10.1016/j.ress.2015.08.016.

[49] B. Una *et al.*, “Simulation of the NuScale SMR and Investigation of the Effect of Load-Following on Component Lifetimes,” *Nucl Technol*, vol. 210, no. 1, pp. 1–22, 2024, doi: 10.1080/00295450.2023.2216973.

[50] M. Wang, X. He, R. Macian-Juan, and X. Wang, “One-dimensional transient analysis of the dual-fluid reactor system,” *Ann Nucl Energy*, vol. 162, Nov. 2021, doi: 10.1016/j.anucene.2021.108481.

[51] H. Shahraki and N. Shabakhty, “Seismic Performance Reliability of RC Structures: Application of Response Surface Method and Systemic Approach,” *Civil Engineering Infrastructures Journal*, vol. 48, no. 1, pp. 47–68, 2015.

[52] J. H. Park, Y. J. An, K. H. Yoo, and M. G. Na, “Leak flow prediction during loss of coolant accidents using deep fuzzy neural networks,” *Nuclear Engineering and Technology*, vol. 53, no. 8, pp. 2547–2555, Aug. 2021, doi: 10.1016/j.net.2021.01.040.

[53] Nuclear Regulatory Commission (NRC), “Westinghouse AP1000 Design Control Document ,” 2011.

[54] J. R. Willis, “Modeling of emergency diesel generators in an 800 megawatt nuclear power plant,” *IEEE Transactions on Energy Conversion*, vol. 8, no. 3, 1993, doi: 10.1109/60.257056.

[55] A. Volkanovski and L. Cizelj, “Nuclear Power Plant Maintenance Optimization with Heuristic Algorithm,” *Science and Technology of Nuclear Installations*, vol. 2014, p. 458016, 2014, doi: 10.1155/2014/458016.

[56] United States Nuclear Regulatory Commission, “Auxiliary Feedwater System,” 2002. Accessed: Mar. 19, 2024. [Online]. Available: https://www.nrc.gov/docs/ML0307/ML030760397.pdf

[57] H. G. Lim, J. E. Yang, and M. J. Hwang, “A quantitative analysis of a risk impact due to a starting time extension of the emergency diesel generator in optimized power reactor-1000,” *Reliab Eng Syst Saf*, vol. 92, no. 7, pp. 961–970, Jul. 2007, doi: 10.1016/J.RESS.2006.07.004.

[58] United States Nuclear Regulatory Commission, “Emergency Diesel Generators,” 2011. Accessed: Mar. 19, 2024. [Online]. Available: https://www.nrc.gov/docs/ML1122/ML11229A061.html

[59] X. Wang, “Draining Time of the Dual Fluid Reactor,” in *12th International Topical Meeting on Nuclear Reactor Thermal-Hydraulics, Operation and Safety (NUTHOS-12)*, 2018. [Online]. Available: https://www.researchgate.net/publication/325846731

[60] M. Ilham and T. Okawa, “A Simple Analytical Model to Predict the Freeze Plug Opening Time in Molten Salt Reactors,” *Journal of Nuclear Engineering and Radiation Science*, vol. 9, no. 4, Jul. 2023, doi: 10.1115/1.4062879.

[61] S. Marchetti, F. Di Maio, and E. Zio, “A Physics-of-Failure (PoF) model-based Dynamic Bayesian Network for considering the aging of safety barriers in the risk assessment of industrial facilities,” *J Loss Prev Process Ind*, vol. 91, p. 105402, Oct. 2024, doi: 10.1016/J.JLP.2024.105402.

[62] L. Miqueles, I. Ahmed, F. Di Maio, and E. Zio, “A Grey-Box Digital Twin-based Approach for Risk Monitoring of Nuclear Power Plants,” 2023. doi: 10.3850/978-981-18-5183-4_s24-05-579-cd.

[63] W. Zhou, “Reliability Evaluation of Corroding Pipelines Considering Multiple Failure Modes and Time-Dependent Internal Pressure,” *Journal of Infrastructure Systems*, 2011, doi: 10.1061/(ASCE).

[64] G. A. Young and T.-L. Sham, “Initial assessment of metallurgical interaction of clad/base metal systems,” Argonne, IL (United States), Sep. 2018. doi: 10.2172/1506992.

[65] Special Metals, “Datasheet of Nickel 201 thermo mechanical properties.” Accessed: May 21, 2024. [Online]. Available: https://www.specialmetals.com/documents/technical-bulletins/nickel-200.pdf

[66] M. Kijima, “Some Results for Repairable Systems with General Repair,” *J Appl Probab*, vol. 26, no. 1, pp. 89–102, 1989, doi: 10.2307/3214319.

[67] M. Kijima, H. Morimura, and Y. Suzuki, “Periodical replacement problem without assuming minimal repair,” *Eur J Oper Res*, vol. 37, no. 2, pp. 194–203, Nov. 1988, doi: 10.1016/0377-2217(88)90329-3.

[68] L. Pinciroli, P. Baraldi, and E. Zio, “Maintenance optimization in industry 4.0,” *Reliab Eng Syst Saf*, vol. 234, Jun. 2023, doi: 10.1016/j.ress.2023.109204.

[69] S. Marchetti, F. Di Maio, and E. Zio, “A Deep Reiforcement Learning method for finding the risk-based optimal prescriptive maintenance policy of degrading safety barriers,” in *The 8th International Conference on System Reliability and Safety (ICSRS)*, 2024.

[70] P. Dömstedt, M. Lundberg, and P. Szakálos, “Corrosion studies of a low alloyed Fe–10Cr–4Al steel exposed in liquid Pb at very high temperatures,” *Journal of Nuclear Materials*, vol. 531, 2020, doi: 10.1016/j.jnucmat.2020.152022.

[71] E. M. Güneyisi and G. Altay, “Seismic fragility assessment of effectiveness of viscous dampers in R/C buildings under scenario earthquakes,” *Structural Safety*, vol. 30, no. 5, 2008, doi: 10.1016/j.strusafe.2007.06.001.

[72] International Atomic Energy Agency (IAEA), “SSG-67 - Seismic Design for Nuclear Installations,” 2021.

[73] International Atomic Energy Agency, “IAEA Safety Standards Series No. SSG-2 (Rev. 1), Deterministic Safety Analysis for Nuclear Power Plants,” 2019.

[74] S. He *et al.*, “A machine learning and CFD based approach for fouling rapid prediction in shell-and-tube heat exchanger,” *Nuclear Engineering and Design*, vol. 432, p. 113759, Feb. 2025, doi: 10.1016/J.NUCENGDES.2024.113759.

[75] M. A. Nasr, L. Loi, S. Riva, A. Zolfaghari, X. Wang, and A. Cammi, “Enhancing multi-physics modeling in new-generation nuclear reactors using machine learning: Implementing Gaussian Process Regression for updating cross sections,” *Ann Nucl Energy*, vol. 224, p. 111720, Dec. 2025, doi: 10.1016/J.ANUCENE.2025.111720.

[76] G. Cataldo, E. Borgonovo, A. Siddens, K. Carpenter, M. Nado, and E. Plischke, “Global sensitivity analyses for test planning with black-box models for Mars Sample Return,” *Risk Analysis*, vol. n/a, no. n/a, Mar. 2025, doi: https://doi.org/10.1111/risa.70010.

[77] L. Pronzato and W. G. Müller, “Design of computer experiments: Space filling and beyond,” *Stat Comput*, vol. 22, no. 3, 2012, doi: 10.1007/s11222-011-9242-3.

[78] B. Auder, A. De Crecy, B. Iooss, and M. Marquès, “Screening and metamodeling of computer experiments with functional outputs. Application to thermal-hydraulic computations,” in *Reliability Engineering and System Safety*, 2012. doi: 10.1016/j.ress.2011.10.017.